Toxicity of polycaprolactone nanoplastics, pristine or weathered in environmental conditions, to human intestinal epithelial cells, in vitro

M. Boulée, V. Bard, M. Papin, D. Béal, S. Devineau, D. Fenel, E. Dusacq, V. Collin-Faure, T. Rabilloud, T. Douki, et al.

Toxicity of polycaprolactone nanoplastics, pristine or weathered in environmental conditions, to human intestinal epithelial cells, *in vitro*

M. Boulée[a], V. Bard[a], M. Papin[a], D. Béal[a], S. Devineau[b,c], D. Fenel[d], E. Dusacq[d], V. Collin-Faure[e], T. Rabilloud[e], T. Douki[a], M. Carriere[a,*]

[a]Univ. Grenoble Alpes, CEA, CNRS, Grenoble INP, IRIG, SYMMES, Grenoble 38000, France.

[b]Université Paris Cité, CNRS, Unité de Biologie Fonctionnelle et Adaptative, 75013 Paris, France.

[c]Université Paris-Saclay, CEA, CNRS, NIMBE, 91191 Gif Sur Yvette, France.

[d]Integrated Structural Biology Grenoble (ISBG), UMS 3518, CNRS, CEA, Université Grenoble Alpes, Grenoble, France.

[e]Univ. Grenoble Alpes, CNRS UMR5249, CEA, IRIG-LCBM, Chemistry and Biology of Metals, F-38054 Grenoble, France.

*Corresponding author: Marie Carriere, SYMMES, 17 rue des Martyrs, Grenoble 38000, France. marie.carriere@cea.fr

Abstract

Plastic, used in almost all everyday products, is a major source of pollution, particularly in the form of micro- and nanoplastics (MNPs). MNP impact on health, particularly on the digestive tract, is still poorly understood, especially in vulnerable populations such as those suffering from inflammatory bowel disease. The aim of this study was to assess the *in vitro* toxicity of nanoplastics (NPLs) from a biodegradable polymer, polycaprolactone (PCL), both in its pristine state and after accelerated weathering in environmental conditions, the latter resulting in the release of potentially toxic PCL oligomers. To do so, we used *in vitro* models of genetic susceptibility to Crohn's disease (CD), consisting in co-cultures of HT29-MTX cells with Caco-2 cells engineered to express either wild-type (WT) or mutated *nucleotide-binding oligomerization domain 2* (NOD2), representative of healthy individuals (Caco-2 $NOD2^{WT}$) or individuals with susceptibility to CD (Caco-2 $NOD2^{1007fs}$). Physicochemical transformation of PCL NPLs upon weathering were characterized. Cells were exposed to pristine and aged PCL NPLs and their cytotoxicity, genotoxicity, inflammatory potential, impact on the cells' redox balance and unfolded protein response, as well as on the epithelial barrier integrity were evaluated. Results show that accelerated weathering increases the crystallinity and leads to fusion of PCL NPLs. PCL NPLs accumulate inside cells where they degrade and release some PCL oligomers. However, in the tested conditions, PCL particles, both pristine and aged, do not show any overt toxicity in both cell systems, irrespective of particle size and weathering status. These data confirm that PCL NPLs, may they be intact or partially dissolved, show only mild toxicity to colon cells, upon acute, short-term exposure of Caco-2 / HT29-MTX cells.

Keywords: Micro and nanoplastics; physicochemical characterization; environmental aging; toxicity; intestinal models; inflammatory bowel disease; polycaprolactone

1. Introduction

Plastic is an essential material, widely used in many sectors due to its advantageous properties and low cost [1]. Its massive production, which exceeded 400 million tonnes (Mt) in 2022, is causing major environmental pollution due to insufficient waste management, with only 10% of plastics being recycled [2, 3]. It is estimated that between 4.8 and 12.7 Mt of plastic waste enter the oceans every year [4]. This situation is exacerbated by plastics' resistance to natural degradation, leading to their accumulation and persistence in the environment for decades to centuries. Once in the environment, exposure of plastic waste undergoes photochemical, mechanical, hydrolytic, thermal and biological stress, which result in the formation of micro- and nanoplastics (MNPs) [5]. Microplastics (MPs) refer to particles smaller than 5 mm, while nanoplastics (NPLs) are generally defined as less than 1 µm, although size definitions vary between studies [6, 7].

Human exposure to MNPs occurs mainly through ingestion or inhalation [8]. The presence of MNPs has been widely reported in drinking water and various food products, including seafood, salt, fish, crustaceans, as well as sugar, honey, and beer [9-11]. Assessing human exposure remains challenging due to the diversity of MNPs and dietary habits. However, a study by Senatirajah et al. estimates that individuals ingest between 0.1 and 5 g of MNPs per week [12], although it is currently recognized as being an overestimation. While a significant proportion of these MNPs is excreted and detected in faeces [13-16], some MNPs can cross biological barriers, reach the bloodstream and some of them have been identified in several human organs as reviewed recently [17]. To date, the health effects of MNPs remain poorly understood, particularly their impact on the digestive tract. In both vertebrates and invertebrates, ingestion of MNPs has been linked to intestinal barrier dysfunction, inflammation and dysbiosis, leading to symptoms similar to those observed in inflammatory bowel diseases (IBD). In zebrafish, exposure to polypropylene (PP) and polystyrene (PS) MNPs induces mucosal damage, increases intestinal permeability, causes dysbiosis and inflammation [18]. In mice, PS MNPs also accumulate in intestinal tissues, disrupting the gut barrier and triggering adverse effects in the intestine and liver, i.e., oxidative stress, inflammation and metabolic disorders, some of these effects being triggered by microbiota dysbiosis [19-21]. *In vitro*, most studies related to MNP toxicity were conducted with PS particles, showing low toxicity except at unrealistically high concentrations, while they heavily accumulate inside intestinal cells [22].

The impact of MNPs on vulnerable populations, particularly individuals with CD, which is one of the most prevalent IBD, remains largely unexplored. While the exact causes of CD are still unclear, the combination of genetic factors, environmental factors and immune system dysfunction has been proposed as playing a role in its development and aggravation, leading to intestinal barrier dysfunction

and abnormal immune responses in the intestine [23]. Yan et al. found a positive correlation between the presence of MNPs in stool of IBD patients and disease severity [15]. Additionally, exposure to PS MNPs exacerbates colitis symptoms in mice with DSS-induced colitis compared to healthy mice [24, 25].

Given the reported adverse effects on health and the environment of non-biodegradable plastics, the development of biodegradable plastics is seen as an attractive alternative due to a shorter half-life in the environment leading to lower exposure [26]. Among these, polycaprolactone (PCL) stands out as a promising biodegradable polyester due to its ability to rapidly decompose through the action of microorganisms or through chemical hydrolysis in various environments [27]. The use of PCL is expanding, particularly for medical and biomedical applications (e.g., resorbable devices and drug-delivery systems) but also for applications such as food packaging, adhesives, agriculture, 3D printing and coatings (for review, see [27]). Although PCL is recognized by the FDA as non-toxic, its prolonged degradation time in the body raises concern about the potential release of oligomers, and about possible toxic effects of both PCL MNPs and oligomers, as some studies have reported that PCL MNPs cause perturbation of epithelial and immune cell normal function [28-30]. Such combination of MNPs and oligomers may be one of the environmental factors contributing to the onset or aggravation of CD, and up to now, although considered as important, the associated toxicity has been overlooked [31, 32].

This work aimed at assessing the toxicological impact of PCL MNPs, either pristine or as a mixture of MNPs and their degradation products, as produced when exposed to environmental conditions, focusing on particles in the sub-micron size range. We previously characterized oligomer release from PCL NPLs upon artificial weathering [33, 34], showing that oligomers ranging from the mono to the hexamer were produced as PCL hydrolyses [33, 34]. Therefore, the first objective of this study was to determine whether weathering-driven changes in particle physicochemical properties, including oligomer release, may contribute to their toxicity. Second, this study aimed at evaluating their impact on the intestine, which was assessed on *in vitro* models of human intestinal epithelium representative of the colon, both healthy and with genetic susceptibility to CD. Traditional *in vitro* models used in toxicology studies related to IBD are models that replicate the active phase of the disease, by inducing inflammation through exposure of Caco-2 cells to strong inflammatory stimuli [35]. Here, we used an *in vitro* model of genetic susceptibility to CD, consisting in Caco-2 cells genetically modified to express either wild-type or mutated *nucleotide-binding oligomerization domain 2* (NOD2). NOD2 plays a crucial role in epithelial cell response to the microbiota and pathobionts by detecting muramyl dipeptide (MDP) from bacterial cell walls, which triggers NF-κB signalling and subsequent inflammatory response [36]. The NOD2 gene is associated with CD, with over 60 identified variants and 30% CD patients

showing one mutation in NOD2. The mutation that is most strongly linked to CD is the 1007fs mutation (NOD2^{1007fs}) [37, 38], which results in a truncated protein that fails to recognize MDP, thus disrupting the NF-κB signalling [39]. Such cell models represent populations at risk of developing CD. Caco-2 NOD2^{WT} and Caco-2 NOD2^{1007fs} cells were co-cultured with the mucus-secreting HT29-MTX intestinal cell line, to reproduce a mucus-secreting ileum-like epithelium [40, 41]. After characterizing the impact of weathering on PCL NPL physicochemical properties, the intracellular accumulation and impact of pristine and weathered PCL NPLs on cell viability, epithelial barrier integrity, ROS intracellular levels, DNA integrity and inflammatory response were assessed. This study provides valuable data related to the toxicological impact of the biodegradable MNPs, namely PCL NPLs and their degradation products, towards intestinal epithelial cells representative of populations at risk of developing CD.

2. Materials and Methods

2.1. PCL particles

PCL NPLs (with diameter 100 nm, 200 nm, 500 nm, or 1000 nm) were purchased from Phosphorex (Hopkinton, USA) as aqueous suspensions and stored at 4°C. These particles are aimed to be used for sustained drug delivery. All the physicochemical characterization and toxicity assays reported in this manuscript were obtained using these non-labelled PCL particles. For cell uptake experiments as assessed via confocal fluorescence microscopy, PCL NPLs were labelled with Disperse Blue 14 (DB14, 1,4-Bis(methylamino)anthraquinone, ABCR #AB177338, λex./λem. 640 nm/685 nm) using the solvent swelling method, leading to NPLs with unchanged size [42, 43]. To this end, a solution of DB14 at 10 mg/mL was prepared in tetrahydrofuran (THF). One percent of this solution (v/v) and 10% THF were added to one volume of particle suspension, and the mixture was stirred on a rotary wheel at room temperature for 30 min. Two volumes of water were then added; then the particles were collected by centrifugation for 30 min at 15,000 x *g*, washed with water and centrifuged again. Finally, the pellet of DB14-labelled NPLs was resuspended in one volume of 20% ethanol.

2.2. Accelerated weathering in a test chamber

To simulate environmental degradation, PCL NPLs were aged in a Q-SUN Xe-1 test chamber (Qlabs) equipped with a xenon arc lamp that reproduces a light spectrum similar to sunlight. The aging conditions were set according to the ISO 4892-2:2013 guideline, which recommends an irradiance of 1.44 W/m²/nm (as measured at 420 nm) and a temperature of 40°C. NPLs were weathered for 96 hours in this condition, under continuous agitation in hermetically sealed quartz cuvettes. A 200 µL aliquot of the suspensions was collected every 24 hours (i.e., at 24, 48, 72, and 96 h) to monitor degradation

over time, which has been reported previously [33, 34]. For the present study, we chose 96h as the degradation duration, as it maximized PCL degradation, while avoiding complete dissolution. The aged suspensions were stored at 4°C until further experiments.

2.3. Physicochemical characterization

2.3.1. Transmission electron microscopy (TEM)

Primary diameters of PCL NPLs were measured on transmission electron microscopy (TEM) images of 100 particles, obtained using negative staining on a grid. PCL NPLs were deposited on the clean side of a carbon film on mica and stained with 2% uranyl acetate or 2% phosphotungstic acid. Then, samples were transferred onto a 400-mesh copper grid and imaged using a Tecnai 12 LaB6 electron microscope equipped with a Gatan Orius 1000 CCD camera, operating at an accelerating voltage of 120 kV and defocus values between 1.2 and 2.5 µm.

2.3.2. Dynamic light scattering (DLS)

Size distributions and polydispersity indexes of 100 µg/mL PCL NPLs suspensions in ultrapure water and in cell culture medium, immediately after dilution and after 24 h of incubation at 37°C, 5% CO_2, at the concentrations used for cell exposure, were assessed by DLS using a Litesizer™ 500 (Anton Paar, USA). Dilution in cell culture medium did not significantly change their size distribution, compared to dilution in water. Surface charge was estimated by measuring the zeta potential using a Univette in a Litesizer™ 500 (Anton Paar, USA). Data were collected and analyzed using the Kalliope™ software.

2.3.3. FTIR and Raman Spectroscopy

FTIR spectra were recorded on particle suspensions that were air-dried on foil, using a Nicolet iS50 spectrometer (Thermo Scientific, USA) equipped with a diamond ATR module. A total of 32 scans were recorded with a resolution of 4 cm^{-1} in the 4000 to 400 cm^{-1} range. FTIR spectra were analyzed using the OMNIC software (Thermo Scientific, USA). Each spectrum represents the average of three measurements recorded on different regions of the sample. Raman spectra were obtained using a WITec alpha300 RA Raman spectrometer (Oxford Instruments, Germany). For this, particles were deposited on a calcium fluoride substrate (ESCO Optics) and spectra were acquired at 532 nm excitation wavelength with a spectral resolution of 0.4 cm^{-1}, via a 100x objective (NA 0.9). The grating was 2400 lines/mm and the laser power was set 10 mW.

2.4. Cell culture and exposure

Caco-2 NOD2^{WT} and Caco-2 NOD2^{1007fs} cells were obtained by transduction of the Caco-2 cell line (ATCC HTB-37, passages 14-40) using a lentivirus expressing either the wild-type NOD2 gene (NOD2^{WT}) or the NOD2 gene carrying the 1007fs mutation (NOD2^{1007fs}). These cell lines were kindly provided by F. Barreau (INSERM U843, Toulouse) and their characterization has been described previously [44, 45]. Mucus-secreting HT29-MTX cells were generously donated by Thecla Lesuffleur (INSERM, Paris) [46]. Cells were seeded in 100 mm Petri dishes (Falcon®) and maintained at 37°C in a 5% CO_2 humidified atmosphere in Dulbecco's Modified Eagle Medium/GlutaMAX™ (DMEM, Gibco™) to which was added 10% decomplemented foetal bovine serum (FBS) (Gibco™), 1% non-essential amino acids (MEM NEAA 100X, Gibco™), 50 units/mL penicillin and 50 µg/mL streptomycin (Sigma-Aldrich™) (complete cell culture medium). Cells were passaged twice a week with Trypsin-EDTA. Co-cultures were established by seeding 90% of Caco-2 NOD2^{WT} or Caco-2 NOD2^{1007fs} cells with 10% of HT29-MTX cells, in multi-well plates at a density of 80,000 cells/cm². They were grown either for 24 h or for 21 days post-confluence to mimic a non-differentiated epithelium or a mature epithelium with tight junctions and microvilli, respectively. Then, they were exposed for 24 h to PCL particles diluted in complete cell culture medium. The tested concentrations were those that are commonly used in toxicological studies, making possible the comparison of our results with those reported in the literature. The highest concentrations, ranging from 12.5 to 200 µg/mL, were used exclusively to assess the impact of the particles on cell viability. For all other assays, lower concentrations (12.5, 25, and 50 µg/mL) were used. Considering a human ingestion of up to 5 g of MNPs per week [12, 47], the human intestine surface being approximately 32 m² [48], it can be estimated that humans are exposed to 0.22 µg MNPs/cm² of intestine per day. We exposed cells to 12.5-50 µg/ml PCL in most experiments, i.e., 3.12-12.5 µg/cm². Therefore, the *in vitro* exposure dose was 15 to 60 time higher than the estimated daily human exposure. This is high, but this can be considered as a worst-case scenario, given that the intestinal transit is not linear and therefore some areas of the intestine may be exposed locally to much higher doses of NPLs than others. Each condition was applied in at least three separate wells (technical replicates) and all tests were repeated independently at least three times with cells at different passage numbers (biological replicates).

2.5. Cell model characterizations

2.5.1. Mucus secretion

The presence of mucus was assessed using Alcian blue staining. Cells were seeded in six-well plates and grown for 21 days, changing the medium every 2-3 days until their differentiation into enterocyte-

like cells [41]. At the end of this differentiation period, cells were washed twice with PBS and fixed for 20 minutes with a mix of 75% ethanol (90°) and 25% acetic acid (3%). Then, a 1% Alcian blue (Sigma-Aldrich, B8438) solution prepared in 3% acetic acid was added to the wells and incubated for 30 minutes at room temperature (RT). Stained cells were observed using a phase contrast microscope (Axiovert 25, Zeiss).

2.5.2. Immunostaining

For immunostaining, cells were seeded in culture chambers on glass slide (Nunc™ Lab-Tek™ II Chamber Slide™ System, Thermo Scientific™). After differentiation, cells were washed with PBS and fixed for 20 min at RT with 4% paraformaldehyde (PFA), then permeabilised for 5 min with 0.2% Triton X-100 and washed three times with PBS. Non-specific proteins were blocked with 3% bovine serum albumin (BSA) for 1 h at RT, then cells were incubated overnight at 4°C with anti-ZO-1 (Sigma-Aldrich, AB2272) or anti-MUC5AC (ABclonal, A17325) primary antibodies. After three washes in 3% BSA, they were incubated with anti-rabbit-IgG Atto 550 antibody (Sigma-Aldrich, 43328) for 2 hours at RT, then washed three times with PBS. After labelling cell nucleus with Hoechst 33342 (Sigma-Aldrich, 14533) for 30 min at RT, samples were washed three times with PBS and coverslips were mounted on slides with Prolong Gold antifade solution (ThermoFisher Scientific). Images were captured using an Olympus IX83 inverted microscope fluorescence microscope and processed with the Fiji software.

2.6. Particle and oligomer cell uptake

First, cellular internalisation of PCL particles was assessed by flow cytometry as previously described [28]. Cells were grown for 24 h in 12-well plates and exposed to 50 µg/mL DB14-labelled PCL particles (PCL-DB14) for 24 h. Then, cells were collected, washed twice with PBS and analyzed by flow cytometry (Melody, Becton Dickinson). Then, PCL particle intracellular accumulation and distribution were also imaged by TEM. Cells were exposed for 24 h to 50 µg/mL PCL particles, then washed twice with 0.1 M PHEM buffer and fixed for 1 h with 2% formaldehyde/0.2 % glutaraldehyde. They were post-fixed with 1% osmium tetroxide to which 1% uranyl acetate was added. Samples were dehydrated with a graded series of ethanol and embedded in Epon resin. The samples were then cut into 1-2 mm strips and embedded a second time in Epon, in the perpendicular orientation, so as, after cutting them, sections allowing observation of the entire thickness of the cells were obtained, i.e., from the apical pole to the basolateral pole. These samples were cut as 80 nm ultrathin sections, which were observed using a JEOL 1200EX TEM operating at 80 kV.

For detection of PCL oligomers (oPCL) within cells, cells were grown in 12-well plates for 24 h, then they were exposed for 24 h or 48 h to 200 µg/mL oPCL standard or 200 nm PCL NPLs. Cells were washed with PBS and harvested using trypsin-EDTA. After washing with PBS, cells were lysed via two freeze-

thaw cycles. Lysates were centrifuged for 10 min at 10,000 x *g* in 0.2 µm filter units and filtrates were analyzed by HPLC-MS/MS as described previously [34]. Samples were injected into a ExionLC AD series chromatographic system (SCIEX, Framingham, MA) equipped with an Nucleodur C18 HiTec column (1.8 µm particle size, 2×100 mm ID, Macherey Nagel, Gutenberg, France). The column oven temperature was set at 50°C and the flow rate was 0.35 ml min^{-1}. The mobile phases were a 2 mM ammonium formate aqueous solution containing 0.1 % formic acid (A) and acetonitrile with 0.1 % formic acid (B). At 0 min, the composition of the gradient was pure A. The proportion of B was then increased to 10 % in 12 min, set to 60 % at 20 min and reached 100 % at 22 min. The latter composition was maintained for 3 min. At the outlet of the column, the flow was directed toward the turbo ion spray source of a 6500+ Qtrap mass spectrometer (SCIEX) operated with the Analyst software (version 1.7, SCIEX). The source temperature was set at 550°C. The pressure of curtain gas, nebulization gas and heated sheath gas were set at 45, 60 and 60 psi respectively. The flow of exhaust gas (air) was set at 25 L min^{-1}. The ion spray voltage was 4500 V. Quantitative analyses of oPCL in aged PCL NPL suspensions were performed in the single ion monitoring (SIM) detection mode, with the $[M-H]^-$ pseudo-molecular ion of each oligomer (monomer to heptamer), used as targeted ions. Quantification in cellular extracts was performed using the multiple reaction monitoring mode (MRM), which is more sensitive. For this purpose, signals corresponding to the fragmentation of targeted pseudo-molecular ions into PCL monomer and dimer were monitored. Quantitative data were inferred from external calibration curves, plotted from standards prepared as follows: pure 6-hydroxyhexanoic acid (6-OH-Hx, 30 mg, Thermo Scientific) was heated for 186 h at 50°C, then 1 mL of ultrapure water was added and the suspension was sonicated for 20 min before being diluted to a concentration of 1 mg/mL. Then, the solution was then filtered analyzed. It was found to contain oPCL carrying between 1 and 6 monomeric units. Their respective proportions were inferred from the total ion current in a HPLC-mass spectrometry analysis.

2.7. Cell viability

PCL particle impact on cell viability was assessed using the WST-1 assay (Roche). Cells were seeded into transparent 96-well plates. They were grown for 24 hours or 21 days after seeding to obtain either non-differentiated or differentiated co-cultures, respectively. Then, cells were exposed to PCL particles for 24 hours. PS-NH_2 50 nm particles (Merck, #L0780) were used as a positive control at either 100 µg/mL (non-differentiated co-cultures) or 500 µg/mL (differentiated co-cultures), since differentiated co-cultures are known to be more resistant to toxic substances due to organization into a tight barrier with microvilli. Therefore, it requires higher concentration of positive control substances to achieve

significant impact [49]. At the end of incubation, the exposure medium was replaced with 100 µL of a 10-fold diluted WST-1 solution prepared in FBS-free medium. After 1.5 hours of incubation, absorbance was measured at 450 nm and corrected for absorbance at 650 nm, using a Spectramax ID3 (Molecular Devices). Results were normalized with respect to the absorbance of control (unexposed) cells.

2.8. Intracellular reactive oxygen species (ROS) level

ROS levels were quantified using the dihydrorhodamine 123 probe (DHR123, Sigma-Aldrich). Twenty-four hours or 21 days after seeding in black 96-well plates, cells were washed with PBS, then exposed for 45 min at 37°C to 1 µM DHR123 prepared in FBS-free medium. Then, the DHR123 solution was replaced with PCL particles and incubated for 24h. Fluorescence was monitored at λexc./λem. 480nm/530 nm, starting immediately after adding the exposure medium to the wells, then after 30 min, 1h, 2h, 4h, 6h and 24h, using the Spectramax ID3 spectrofluorometer. Data are expressed as % of the fluorescence value of control (unexposed) cells. Tert-butyl hydroperoxide (TBHP, Sigma-Aldrich, 1 mM) was used as positive control.

2.9. DNA damage

DNA strand breaks were quantified using the comet assay in alkaline condition, without formamidopyrimidine-DNA glycosylase (FPG) treatment. Cells were seeded in 12-well plates and exposed to PCL particles after 24 h or 21 days of differentiation. Methyl methanesulfonate (MMS, 30 µg/mL) was used as positive control. At the end of the treatment, cells were washed with PBS and harvested using trypsin-EDTA. Cells were washed with PBS and stored at -80°C in a cryoprotective solution (85.5 g/L sucrose, 11.76 g/L sodium citrate and 50 mL/L DMSO, pH 7.6), as such storage has been shown to preserve DNA integrity [50]. Glass slides were coated with 1% agarose and allowed to dry. Then, exposed cells were mixed with 1% low-melting agarose and deposited on the slides as two 70 µL gels per slide. After gel solidification, cells were lysed for 1 h in 2.5 M NaCl, 10 mM Tris, 0.1 M EDTA and 1% Triton X-100, pH 10 to release the DNA, then washed 3 times with PBS. Slides were immersed in cold electrophoresis buffer (0.3 M NaOH, 1 mM EDTA, pH > 13) and incubated for 40 min, allowing the DNA to unwind. Then, a 1.2 V/cm current was applied to the slides for 30 min, to allow DNA migration. The slides were washed twice for 10 minutes in PBS and labelled for 20 min with 25 µL GelRed™ (Biotium) diluted 1,000-fold in PBS. Comets were imaged on an Axioskop fluorescence microscope (Zeiss) and analyzed using Comet Assay IV (Perceptive Instruments). Fifty comets per gel

were analyzed, randomly chosen. The median value of % tail DNA was measured out of these 50 comets. Each condition yielded six values (three technical replicates, with two gels for each of them), which were averaged.

2.10. Intestinal barrier integrity (TEER and fluorescein passage)

For TEER measurements, cells were grown on polyester Transwell-clear inserts with a 0.4 µm pore size (Costar, #3460) and maintained for 21 days post-confluence. Their culture medium was changed three times per week. TEER was monitored over these 21 days using an EVOM3 epithelial volt/ohm meter equipped with an ENDOHM-12 electrode (World Precision Instruments). After 21 days, cells were exposed to PCL particles for 24 hours, then the TEER of each insert was measured. EDTA (ethylenediaminetetraacetic acid, 2 mM) was used as positive control. The TEER from a blank insert (without cells) was subtracted to the measured values. The obtained values are expressed as % of the TEER of control (unexposed) cells. Following this, the exposure medium was replaced with medium containing 5 µg/mL fluorescein (Sigma-Aldrich). After 2 h of incubation, 100 µL of apical medium and 100 µL of basolateral medium were transferred to a black 96-well plate and fluorescence was measured on a Spectramax ID3 spectrofluorometer (Molecular Devices) at λexc./λem. 460 nm/515 nm. Results were expressed as % fluorescence of control (unexposed) cells.

2.11. Inflammation

Secretion of IL-8 was assessed by ELISA (Invitrogen, #88-7066-88). Cells were seeded in 12-well plates, grown for 24 h, then exposed for 24 h to PCL particles. At the end of exposure, exposure medium was harvested and stored at -80°C. A transparent 96-well plate was incubated overnight at 4°C with the capture antibody, diluted in 0.1 M sodium carbonate. Then, the wells were washed three times with wash buffer (PBS 1X, 0.05% Tween®20) and non-specific binding sites were blocked for 1 h with 10% decomplemented FBS prepared in PBS. A standard range was prepared using the IL-8 powder from the kit. After washing the plate three times, the standards and supernatants were deposited in the wells and incubated for 2 h at RT. After five washes, the detection antibody was added and incubated for 1 h at RT. After five washes, the detection enzyme (peroxidase) was added and incubated for 30 min, followed by seven washes. Finally, the TMB substrate (3,3', 5,5' tetramethylbenzidine) was incubated for 30 min at RT in the dark. The reaction was stopped by adding 1 M sulphuric acid (H_2SO_4). Absorbance was measured at 450 nm using a Spectramax ID3 (Molecular Device), with a background

correction at 570 nm. Absorbances values were converted to concentration using the IL-8 calibration curve.

2.12. Reverse transcription-quantitative polymerase chain reaction (RT-qPCR)

The impact of PCL particles on mRNA expression was assessed by RT-qPCR, targeting genes involved in oxidative stress, inflammation, endoplasmic reticulum stress, mucin secretion and xenobiotic efflux. Cells were seeded in 12-well plates and allowed to grow for 24 h. Then, they were exposed for 24 h to 100 or 200 nm PCL particles. At the end of the treatment, cells were washed with PBS, lysed and their mRNA was extracted according to the supplier's protocol (NucleoSpin RNA, MACHEREY NAGEL, 740955). It was reverse transcribed using SuperScript™ III (Invitrogen, 18080093). For qPCR, a reaction mix consisting of 20 ng of cDNA, 12.5 µL of Takyon No ROX SYBR MasterMix blue dTTP (Eurogentec), 2.5 µL of 2 µM sense and antisense primers and nuclease-free water was prepared in a final volume of 25 µL and deposited in the wells of a white 96-well qPCR plate. The plate was sealed with adhesive film, centrifuged for 5 min at 700 x *g*, and analysed using a CFX96 Touch Real-Time PCR Detection System (Biorad) with the following thermal cycle: 95°C for 5 min, 40 cycles of amplification 95°C for 15 s, 55°C for 20 s, and 72°C for 40 s, then the melting curve: 95°C for 1 min, 55°C for 30 s, and 95°C for 30 s. Results were analysed using REST© 2009 software [51]. The reference genes were glyceraldehyde-3-phosphate dehydrogenase (GAPDH) and cyclophilin B (CycloB). Their sequences, as well as those of mRNA-specific primers, are reported in Table S1. Primer efficiency was tested prior to the experiment, being equal to 2 ± 0.3.

2.13. Statistical analysis

In all experiments except RT-qPCR, due to the small number of replicates in the experiments, data did not follow a normal distribution, variances were not homogeneous and the condition of homoscedasticity of residuals was not met. As a result, non-parametric statistical tests were carried out, i.e., Kruskal-Wallis tests, followed by two-tailed Dunn's post-hoc tests, using GraphPad Prism version 7. Results are considered statistically significant (*) when the p-value is less than 0.05.

3. Results

3.1. Artificial weathering and physicochemical characterization

According to the manufacturer's information, PCL particle diameters were 100, 200, 500 and 1000 nm. TEM analysis revealed that these particles were spherical but exhibited a rather heterogeneous size distribution. The measured primary diameters were 78 ± 22 nm, 204 ± 87 nm, 505 ± 182 nm and 939 ± 275 nm, respectively (Figure 1A-D).

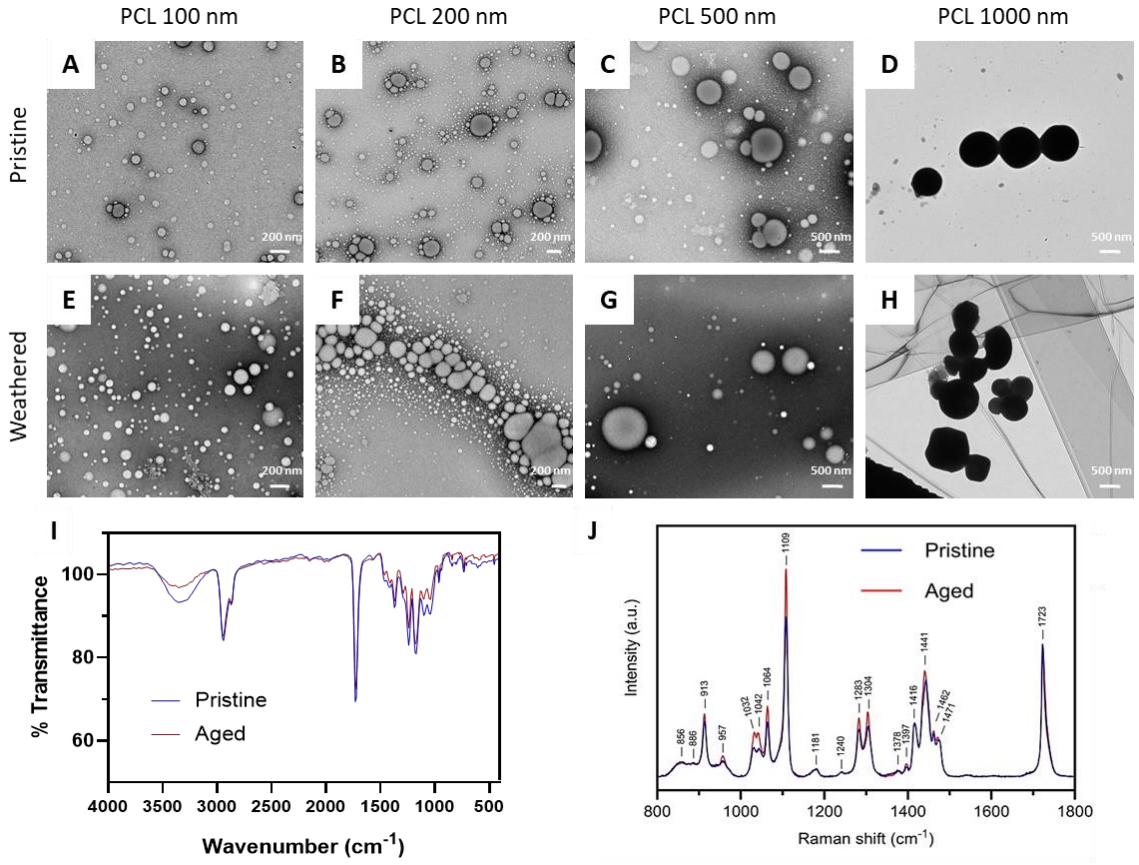

Figure 1. Physicochemical characterization of pristine and aged PCL particles. (A-H) TEM observations of pristine (A-D) and aged (E-H) PCL particles with diameter 100 nm (A, E), 200 nm (B, F), 500 nm (C, G) and 1000 nm (D, H). FTIR (I) and Raman (J) analysis of pristine (blue spectrum) and aged (red spectrum) 200 nm PCL particles.

These observations were confirmed by DLS analysis, which showed mean Z-averages of 105 ± 5 nm and 197 ± 2 nm for the 100 and 200 nm particles, respectively, while their polydispersity index (PdI) was 0.17 (Table 1; size distributions are presented in Figure S1). This suggests size heterogeneity but mild agglomeration. Regarding 500 nm particles, the Z-average was 363 ± 60 nm (PdI 0.14 ± 0.07), which was significantly smaller than in the TEM measurement, likely due to the formation of aggregates exceeding 1 µm. Such large particles are known to hamper proper measurement of smaller particles. The Z-average of 1000 nm particles could not be determined using this technique, which is

not well suited to measure particles with diameters > 1µm. PCL NPLs exhibited a slightly negative zeta potential (Table 1). Following artificial weathering, morphological changes were observed, including fusion of some of the particles which appeared less spherical (Figure 1E-F). However, particle fusion was not frequent and did not lead to significant changes in primary diameter, Z-average or polydispersity index, except for the 100 nm and 500 nm particles, for which the primary diameter was 15% larger (100 nm PCL NPLs) and 10% smaller (500 nm PCL NPLs) compared to the respective pristine PCL NPLs (Table 1 and Figure S1). A slight decrease in zeta potential was observed; however, this trend was not statistically significant (Table 1).

Table 1. Physico-chemical characteristics of pristine and weathered PCL particles[a]

	PCL 100 nm	PCL 200 nm	PCL 500 nm	PCL 1000 nm
Primary diameter (nm)				
Pristine (mean ± s.d.)	78±22	204±85	505±182	939±275
Pristine (50th [10th-90th] percentile)	73 [54-106]	190 [114-319]	473 [313-723]	881 [648-1239]
Aged (mean ± s.d.)	92±43*	192±79	458±314*	937±267
Aged (50th [10th-90th] percentile)	83 [52-148]	176 [120-276]	321 [168-911]	939 [571-1234]
Z-average (nm)				
Pristine	105±5	197±2	363±60	*n.a.*
Aged	102±2	186±4	387±13	*n.a.*
Polydispersity index				
Pristine	0.17±0.03	0.17±0.05	0.14±0.07	*n.a.*
Aged	0.12±0.02	0.17±0.04	0.24±0.01	*n.a.*
Zeta (mV)				
Pristine	-3.3±3.9	-10.4±1.1	-7.8±4.4	-7.1±4.5
Aged	-8±2.5	-14.8±1.9	-18.5±0.3	-14.8±0.8

[a] Primary diameter was determined from TEM observations (n=100), Z-averages and polydispersity indexes (PdI) were obtained from DLS analysis (n=3), zeta potential (Zeta) from ELS analysis (n=3). Statistical significance: *p<0.05, aged vs. pristine.

The chemical composition of PCL NPLs was confirmed via FTIR and Raman analysis. Indeed, the FTIR spectrum recorded on 200 nm PCL particles revealed the characteristic features of PCL (Figure 1I). These features included bands at 2944 cm^{-1} and 2867 cm^{-1}, corresponding to the asymmetric and symmetric stretching of CH_2 groups, as well as ester-specific bands, particularly at 1723 cm^{-1}, attributed to the ester carbonyl (C=O) stretching, and at 1240 cm^{-1} and 1186 cm^{-1}, corresponding to asymmetric and symmetric stretching of the C-O-C group. Weathering did not significantly change these FTIR spectrums, as no new peak emerged and no characteristic peak disappeared. FTIR spectrums for 100 nm, 500 nm and 1000 nm PCL particles, reported in Figure S2, led to similar conclusions. Raman analysis of 200 nm PCL NPLs revealed some changes in characteristic peaks after weathering, compared to pristine NPLs. These changes included variations in the intensity of crystalline peaks at 913, 1032-1109, 1283-1304, and 1416-1471 cm^{-1}, corresponding to the C-COO stretching, C-C backbone stretching, CH_2 twisting, and CH_2 bending, respectively (Figure 1J).

3.2. Characterization of cell models

The phenotypic characterization of Caco-2 NOD2^{WT} and Caco-2 NOD2^{1007fs} has been described elsewhere [45]. In this study, the used cell models were co-cultures of these cells with HT29-MTX mucus-secreting cells. Such co-cultures were used either non-differentiated, i.e., exposed 24h after seeding, which is representative of a proliferative epithelium, or differentiated via growing them 21 days post-confluence, which triggers their differentiation into a mature intestinal epithelium with tight junctions and microvilli [41]. Traditionally, Caco-2/HT29-MTX cell differentiation is performed on cells growing on semi-permeable inserts such as Transwell inserts. In the present study, they were grown on plastic or glass, therefore their differentiation status on these surfaces was examined.

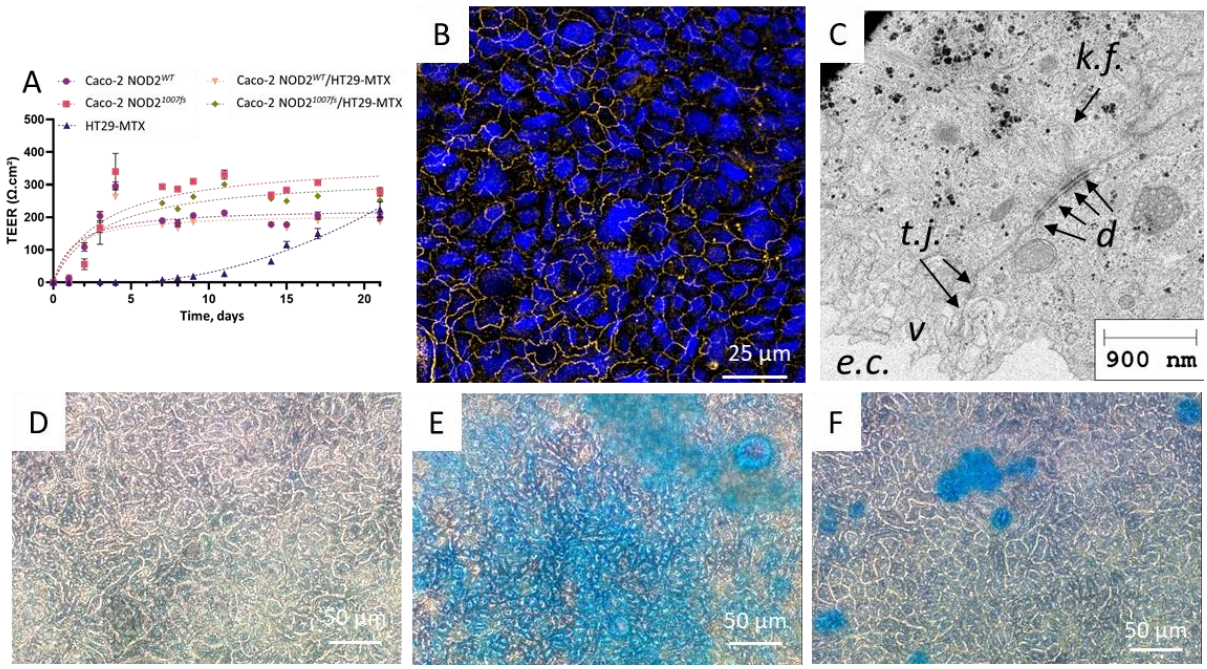

Figure 2. Characterization of differentiated Caco-2 NOD2$^{WT\ or\ 1007fs}$/HT29-MTX. Assessment of epithelium differentiation via measurement of the transepithelial electrical resistance (TEER) throughout the differentiation period (A). ZO-1 immunostaining of Caco-2 NOD2^{WT}/HT29-MTX after 21 days of differentiation (B). TEM image of Caco-2 NOD2^{WT}/HT29-MTX exposed to 200 nm PCL NPLs (C), showing the presence of tight junctions (t.j.) and desmosomes (d) with associated keratin fibres (k.f.), as well as microvilli (v), which are hallmarks of epithelial cell differentiation. Mucus secretion visualized by Alcian blue staining in Caco-2 NOD2^{WT} (D), HT29-MTX (E) and Caco-2 NOD2^{WT}/HT29-MTX (F).

Differentiation into a tight epithelium was proven through TEER measurements and ZO-1 immunostaining. After 21 days of culture post-confluence, Caco-2 NOD2^{WT} exhibited a TEER of 199 ± 11 Ω.cm², whereas the Caco-2 NOD2^{WT}/HT29-MTX co-culture showed a slightly lower resistance, reaching 187 ± 5 Ω.cm² (Figure 2A). Similarly, the TEER of Caco-2 NOD2^{1007fs} was 278 ± 14 Ω.cm², while that of the Caco-2 NOD2^{1007fs}/HT29-MTX co-culture was 252 ± 3 Ω.cm² (Figure 2A). Lower TEER of co-

cultures, as compared to monocultures, may be attributed to the presence of HT29-MTX cells, which show a much lower TEER compared to Caco-2 cells (Figure 2A).

ZO-1 immunostaining showed a uniform and continuous distribution along cell edges, indicating the presence of tight junctions (Figure 2B). Cells showed tight junctions, desmosomes and associated keratin fibres, as well as microvilli as observed by TEM (Figure 2C). Overall, this confirms that Caco-2 NOD2^{WT}/HT29-MTX differentiate into a tight epithelium, even when grown on plastic dishes rather than on transwell inserts. Mucus secretion was monitored by Alcian blue staining (Figure 2D-F). As expected, Caco-2 NOD2^{WT} monoculture (Figure 2D) was negative for Alcian blue staining, indicating the absence of mucus secretion. In contrast, HT29-MTX monoculture (Figure 2E) and Caco-2 NOD2^{WT}/HT29-MTX co-culture (Figure 2F), produced a significant amount of mucus. Mucus covered HT29-MTX cell monoculture, but was not homogeneously distributed on top of the co-culture, likely locating only above HT29-MTX cells. The same was observed with Caco-2 NOD2^{1007fs} cells (Figure S3A-B). Immunostaining showed cytoplasmic distribution of MUC5AC, specifically expressed by HT29-MTX cells (Figure S3C).

3.2. Internalization and accumulation of PCL particles and oligomers

Next, cells were exposed to PCL particles for accumulation and toxicity assessments. Throughout this study, we expressed the exposure concentration on a mass basis (µg/mL of exposure medium). Table S2 shows the corresponding concentration as number of particles per exposed well or as number of particles per cell, as calculated based on their size distribution.

Cellular accumulation of PCL particles was first assessed using flow cytometry, using 200 nm DB14-PCL fluorescently-labelled particles. After gating cells appropriately (Figure S4A), Control cells showed very low fluorescence (Figure S4B), while fluorescence of both Caco-2 NOD2^{WT}/HT29-MTX (Figure S4C, S4E, S4G) and Caco-2 NOD2^{1007fs}/HT29-MTX (Figure S4D, S4F, S4H) increased with respect to exposure concentration, reflecting increased DB14-PCL intracellular accumulation. The mean fluorescence intensity (MFI) shifted from 1.8 ± 0.7 fluorescence units (fu) in control (unexposed) cells to 33.5 ± 1.6 fu, 56.4 ± 0.3 fu, 65.5 ± 0.6 fu in Caco-2 NOD2^{WT}/HT29-MTX cells exposed to 25, 50 or 100 µg/mL DB14-PCL, respectively (Table 2). MFI in Caco-2 NOD2^{1007fs}/HT29-MTX cells increased from 1.4 ± 0.3 fu in control cells to 35.9 ± 0.8 fu, 53.8 ± 2.1 fu and 59.9 ± 1.4 fu in cells exposed to 25, 50 or 100 µg/mL DB14-PCL, respectively (Table 2), which did not significantly differ from the respective fluorescence of Caco-2 NOD2^{WT}/HT29-MTX.

455 Table 2. Flow cytometry analysis of PCL-DB14 accumulation in Caco-2 / HT29-MTX cells[a]

PCL-DB14 concentration	Caco-2 NOD2^{WT} / HT29-MTX	Caco-2 NOD2^{1007fs} / HT29-MTX
0	1.8 ± 0.7	1.4 ± 0.3
25 µg/mL	33.5 ± 1.6*	35.9 ± 0.8*
50 µg/mL	56.4 ± 0.3*,#	53.8 ± 2.1*,#
100 µg/mL	65.5 ± 0.6*,#	59.9 ± 1.4*,#

456 [a] Mean fluorescence intensity (MFI) of cells exposed for 24 h to 25, 50 or 100 µg/mL PCL-DB14. Statistical significance:
457 *p<0.05, exposed vs. control; #p<0.05, 50 µg/mL vs. 25 µg/mL or 100 µg/mL vs. 50 µg/mL; $p<0.05 Caco-2 NOD2WT / HT29-
458 MTX vs. Caco-2 NOD21007fs / HT29-MTX: no statistical significance within these comparisons.

459 Then, PCL particle intracellular accumulation was probed by TEM imaging, confirming that PCL particles
460 accumulated in cells and located only in the cytoplasm, where they distributed in cytoplasmic vesicles
461 throughout the cells (Figure 3). PCL NPLs appeared light grey in these vesicles, because polymers are
462 not stained by osmium tetroxide and uranyl acetate. They showed spherical morphology and size
463 heterogeneity, which reflect the heterogenous size distribution of the used PCL particles as already
464 commented in section 3.1. No particle was observed in the cell nucleus or mitochondria in any of the
465 observed regions of the samples. The type of vesicles in which particles accumulated could not be
466 determined unambiguously, still they were always surrounded by a membrane and their relatively high
467 electron-density suggests that they were probably lysosomes.

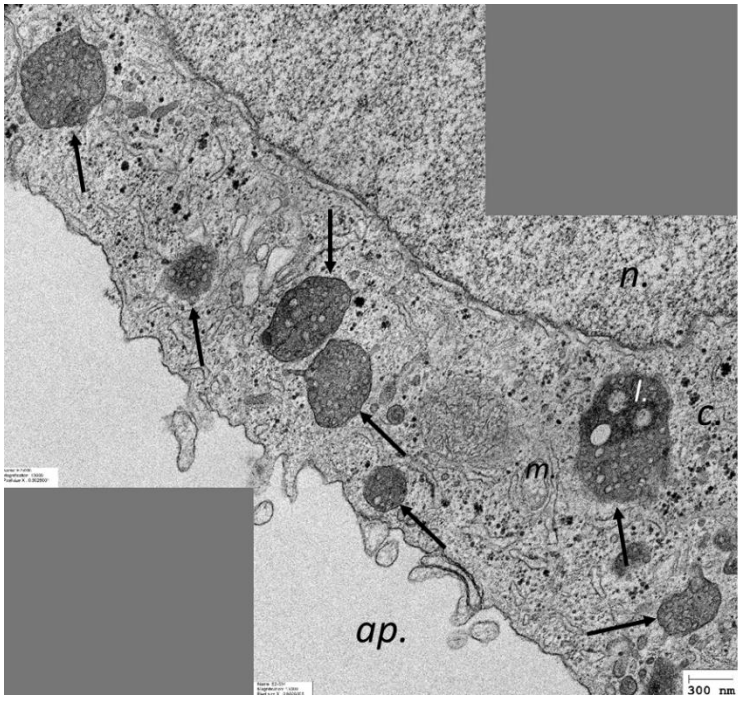

468

469 **Figure 3.** TEM image of a Caco-2 NOD2^{WT}/HT29-MTX cell exposed to 200 nm PCL particles. Two images are merged as a single
470 image, explaining why some grey regions are visible top right and down left corners of the image. Cells were exposed to 50
471 µg/mL of 200 nm pristine PCL NPLs for 24 h. This image shows the apical pole of the cell (*ap*.), with PCL particles accumulated

in electron-dense vesicles resembling lysosomes (arrows, *l.*) in the cell cytoplasm (*c.*). No PCL particle was observed in any of the observed cell nucleus (*n.*) or mitochondria (*m.*).

Anticipating the intracellular hydrolysis of internalized PCL particles, especially as they were accumulated in lysosomes where the pH is low and that contain a variety of enzymes aiming at degrading xenobiotics, we developed a HPLC-MS/MS method to quantify PCL oligomers in cell lysates, based on a highly sensitive multiple reaction monitoring (MRM) detection. Figure 4 illustrates PCL oligomer quantification in extracts from Caco-2 NOD2^{WT}/HT29-MTX cells exposed for 24 or 48 hours to 200 nm PCL particles. As a comparison, cells were also exposed to a mixture of synthetic PCL oligomers (oPCL). The amount of oPCL to which cells were exposed corresponded to the amount of oligomers that would be released by the particles if they totally dissolved, as calculated according to their previously observed acellular dissolution behaviour [33]. Cells heavily accumulated oPCL, and intracellular accumulation increased as exposure time increased (Figure 4A). Intracellular oligomers could also be detected in cells exposed to PCL particles, although in quantities more than one order of magnitude lower than in cells exposed to oPCL. Their intracellular level remained stable over time (Figure 4A). With respect to oligomer length, the proportion of monomer, dimer, trimer and other polymer lengths differed in cells exposed to PCL particles, compared to cells exposed to oPCL. In cells exposed to PCL particles, after 24 h of exposure the same amount of monomer and trimer could be observed, as well as approximately half this amount of dimer. Some tetramers and pentamers could also be detected, although in minute quantities (Figure 4B). After 48h of exposure, the level of tetramers and pentamers decreased while the concentration of monomer increased, reaching 1.5-fold its amount at 24 h (Figure 4B). In cells exposed to oPCL, only monomers and dimers were detected at 24 h, the monomer being predominant (Figure 4C). At 48h post-exposure, the amount of dimer decreased and the amount of monomer increased, suggesting that the dimer degraded inside the cells to form some monomers (Figure 4C).

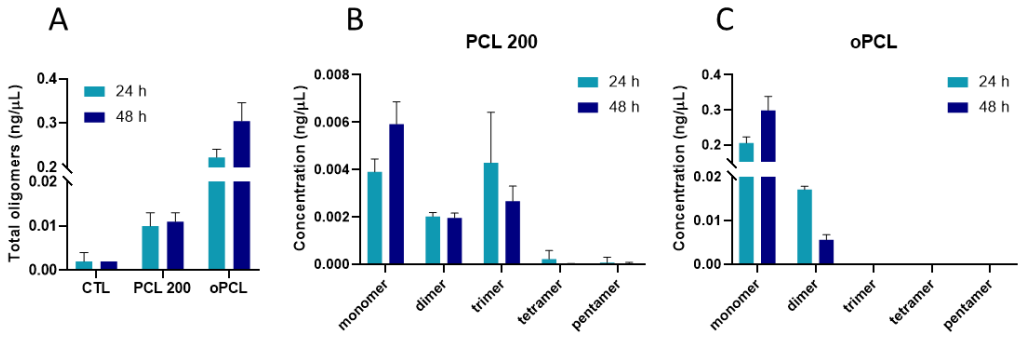

Figure 4. Quantification of PCL oligomers in Caco-2 NOD2^{WT}/HT29-MTX extracts. Cells were exposed for 24 h or 48 h to 200 nm pristine PCL NPLs (PCL200) (A, B) or to synthetic PCL oligomers (oPCL) (A, C). Cells were washed, then lysed, and PCL oligomers were quantified by HPLC-MS/MS in the filtered lysate. Mean ± standard deviation.

3.3. Toxicity towards non differentiated Caco-2 NOD2^{WT}/HT29-MTX or NOD2^{1007fs}/HT29-MTX

First, the toxicity of PCL particles was tested on Caco-2 NOD2^{WT}/HT29-MTX and NOD2^{1007fs}/HT29-MTX 24 h after their seeding, i.e., in a condition where they are still proliferative and not differentiated as mature enterocytes. This mimics proliferative cells at the vicinity of intestinal crypts. When assessed using the WST-1 assay, pristine (Figure 5A-B) and aged (Figure 5C-D) PCL particles did not alter the viability of non-differentiated Caco-2 NOD2^{WT}/HT29-MTX (Figure 5A, C) and Caco-2 NOD2^{1007fs}/HT29-MTX (Figure 5B, D), irrespective of their size and concentration. Similarly, PCL oligomers did not induce cell death at the tested concentrations (Figure 5C-D). Moreover, neither pristine nor aged PCL particles, regardless of their size, caused any increase in intracellular reactive oxygen species (ROS) levels in non-differentiated Caco-2 NOD2^{WT}/HT29-MTX (Figure 6A) or Caco-2 NOD2^{1007fs}/HT29-MTX (Figure 6B) after 24 h of exposure. A statistically significant decrease in fluorescence was observed, especially with 200 nm and 1000 nm PCL particles. This decrease was very weak, which questions its physiological relevance. Figure S5 shows the monitoring of intracellular ROS from 30 minutes to 24 hours post-exposure, showing no significant difference in exposed cells, compared to control cells, regardless of the timepoint, cell model or particle type, i.e., pristine or aged.

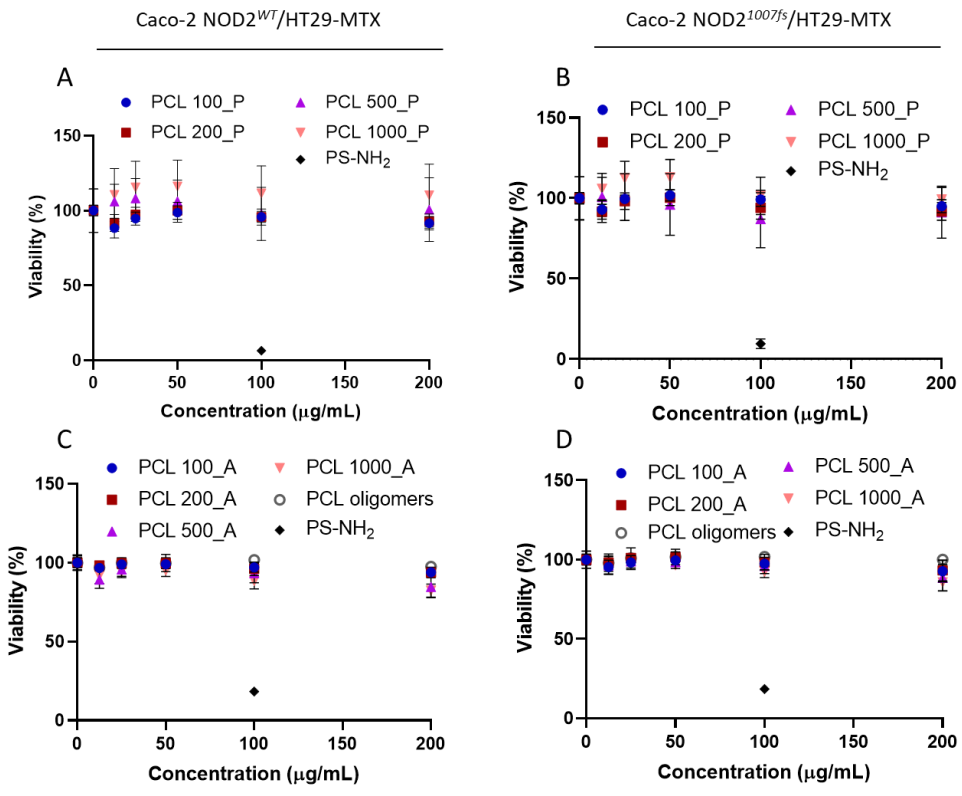

Figure 5. Cytotoxicity of PCL particles and PCL oligomers to non-differentiated Caco-2 / HT29-MTX cells. Cytotoxicity was assessed using the WST-1 assay in non-differentiated cells, i.e., 24 h after seeding, exposed for 24 h to pristine (A-B) or aged (C-D) PCL particles or oligomers, on Caco-2 NOD2^{WT}/HT29-MTX (A, C) and Caco-2 NOD2^{1007fs}/HT29-MTX (B, D). PS-NH$_2$ (50

nm, 100 µg/mL) were used as positive control. Results are expressed as % relative to control (unexposed cells). Mean ± standard deviation.

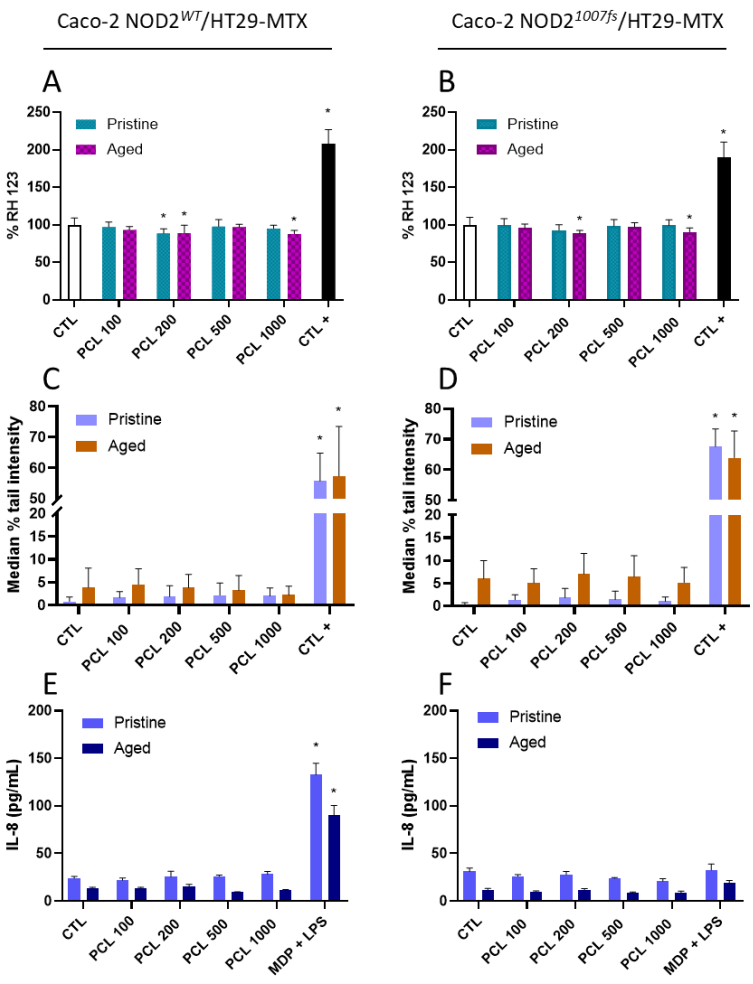

Figure 6. Impact of PCL particles on intracellular ROS levels, DNA integrity and IL-8 secretion in non-differentiated Caco-2 / HT29-MTX cells. Caco-2 NOD2^{WT}/HT29-MTX (A, C, E) and Caco-2 NOD2^{1007fs}/HT29-MTX (B, D, F) were exposed for 24 h, 24 h post-seeding, to 50 µg/mL pristine or aged PCL NPLs. Intracellular ROS levels were quantified using the DHR123 probe (A-B), genotoxicity via the comet assay in alkaline conditions (no Fpg) (C-D) and inflammation by monitoring IL-8 secretion in the exposure medium (E-F). Tert-butyl hydroperoxide (1 mM), methyl methanesulfonate (30 µg/mL) and a mixture of 10 µg/mL MDP and 2 µg/mL LPS were used as positive controls (CTL+) in the DHR123, comet and IL-8 quantification assays, respectively. Mean ± standard deviation; statistical significance: *p<0.05, exposed vs CTL.

These results are consistent with the RT-qPCR analysis of gene expression, which showed no alteration of the mRNA expression of genes involved in oxidative stress regulation, i.e., CAT, SOD1, SOD2, GCLM and HO-1 (Table 3). The only observed changes were SOD-1 and GCLM mRNA expressions, which were decreased in Caco-2 NOD2^{WT}/HT29-MTX exposed to pristine 200nm PCL particles, as well as SOD-2 and HO-1 mRNA expression that was slightly increased in Caco-2 NOD2^{1007fs}/HT29-MTX exposed to 100 nm pristine PCL particles (Table 3). This suggests homeostatic regulation, which did not lead to overt oxidative stress as no excess ROS were detected.

Table 3. RT-qPCR analysis of mRNA expression in non-differentiated Caco-2 NOD2^{WT}/HT29-MTX and Caco-2 NOD2^{1007fs}/HT29-MTX cells[a]

	WT				1007fs			
	100 nm pristine	100 nm aged	200 nm pristine	200 nm aged	100 nm pristine	100 nm aged	200 nm pristine	200 nm aged
Ox. stress								
CAT	-	-	-	-	-	-	-	-
SOD1	-	-	0.52±0.10	-	-	-	-	-
SOD2	-	-	-	-	-	-	-	-
GCLM	-	-	0.59±0.10	-	-	-	-	-
HO-1	-	-	-	-	1.76±0.51	-	-	-
Inflammation								
IL-1β	-	-	-	-	-	-	-	-
IL-8	-	-	1.93±0.38	-	-	-	-	-
TNFα	-	-	-	-	1.88±0.51	-	-	-
ER stress								
ATF6	1.56±0.24	1.69±0.27	1.30±0.19	2.02±0.51	-	-	-	-
GRP78	-	-	-	-	3.00±0.88	3.37±0.86	-	2.53±0.78
IRE1	-	-	-	-	1.85±0.49	-	-	-
sXBP1	-	-	-	-	1.83±0.55	-	-	-
CHOP	-	-	-	-	2.50±0.65	2.71±0.66	-	2.04±0.53
Mucins								
MUC2	-	-	0.51±0.10	0.32±0.07	-	-	-	-
MUC5AC	-	-	0.71±0.13	-	-	-	-	-
Efflux pumps								
MDR1	-	-	-	1.77±0.36	-	-	-	-
MRP1	1.39±0.17	-	-	-	-	-	-	-
MRP2	-	-	-	-	-	-	-	-
BCRP	-	-	-	-	-	-	-	-

[a]mRNA expression normalized using the ΔΔCt method, analysed in Caco-2 NOD2^{WT}/HT29-MTX cells (WT) and in Caco-2 NOD2^{1007fs}/HT29-MTX cells (1007fs), exposed to 50 µg/mL of 100 nm or 200 nm PCL particles, pristine or aged. Only statistically significant results are reported, non-significant data are represented by a dash. Absolute gene regulation ± standard error, as calculated using REST2009 [51].

Similarly, no significant increase of DNA strand breaks and/or alkali-labile sites was observed in non-differentiated cultures of Caco-2 NOD2^{WT}/HT29-MTX (Figure 6C, 50 µg/mL and Figure S6, all tested concentrations) and Caco-2 NOD2^{1007fs}/HT29-MTX (Figure 6D, 50 µg/mL and Figure S6, all tested concentrations), exposed to pristine or aged PCL particles, whatever their diameter. Finally, no significant increase in IL-8 secretion was observed after exposure of non-differentiated Caco-2 NOD2^{WT}/HT29-MTX (Figure 6E, 50 µg/mL and Figure S7, all tested concentrations) and Caco-2 NOD2^{1007fs}/HT29-MTX (Figure 6F, 50 µg/mL and Figure S7, all tested concentrations) to PCL particles, pristine or aged, whatever their size. Conversely, co-exposure to MDP at 10 µg/mL and LPS at 2 µg/mL induced IL-8 secretion in Caco-2 NOD2^{WT}/HT29-MTX but not in Caco-2 NOD2^{1007fs}/HT29-MTX cells. It was expected since MDP is the natural ligand for NOD2, and NOD2 does not recognize MDP when carrying the 1007fs mutation. At the mRNA expression level, signs of inflammation were observed only in Caco-2 NOD2^{WT}/HT29-MTX exposed to pristine 200 nm PCL particles, where IL-8 mRNA expression

was significantly increased (Table 3) and in Caco-2 NOD2^{1007fs}/HT29-MTX exposed to pristine 100 nm PCL, where increased mRNA expression of TNF-α was measured (Table 3).

Finally, the impact of PCL NPLs on the expression of mRNAs encoding proteins involved in the response to endoplasmic reticulum (ER) stress, i.e., the unfolded protein response (ATF6, GRP78, IRE1, sXBP1 and CHOP), mucin secretion (MUC2 and MUC5AC) and xenobiotic efflux pumps belonging to the ABC transporter family (MDR1, MRP1, MRP2 and BCRP) was analyzed by RT-qPCR. All mRNA relative expression results are reported in Table 3. The most affected pathway was ER stress, with ATF-6 mRNA expression that was increased in all tested conditions in Caco-2 NOD2^{WT}/HT29-MTX, whereas in Caco-2 NOD^{1007fs}/HT29-MTX pristine 100 nm PCL particles significantly increased GRP78, IRE1, sXBP1 and CHOP mRNA expression. GRP78 and sXBP1 mRNA expression was also increased in Caco-2 NOD^{1007fs}/HT29-MTX exposed to aged 100 nm and 200 nm PCL particles. Moreover, mRNA expression of some xenobiotic efflux pumps was also significantly affected, with MRP1 expression that was increased in Caco-2 NOD2^{WT}/HT29-MTX exposed to 100 nm or 200 nm pristine PCL particles, while MDR1 expression was also increased in Caco-2 NOD2^{WT}/HT29-MTX exposed to 200 nm pristine PCL particles. No significant change was observed in Caco-2 NOD2^{1007fs}/HT29-MTX cells. In the mucus secretion pathway, no significant change was observed in Caco-2 NOD2^{1007fs}/HT29-MTX cells, while pristine 100 nm PCL increased the mRNA expression of MRP1 and aged 200 nm PCL particles increased the mRNA expression of MDR1 in Caco-2 NOD2^{WT}/HT29-MTX.

3.4. Toxicity towards differentiated Caco-2 NOD2^{WT} or NOD2^{1007fs}/HT29-MTX

Then, the toxicity of PCL particles was assessed on differentiated Caco-2/HT29-MTX cells, in which Caco-2 cells are differentiated into mature enterocytes with tight junctions and villi, therefore being more representative of human intestinal epithelium. Differentiated Caco-2/HT29-MTX cells are known to be more resistant to particles than undifferentiated ones, owing to the presence of microvilli that would hamper particle uptake by endocytosis. Pristine and aged PCL, whatever their size, did not affect the viability of differentiated Caco-2 NOD2^{WT}/HT29-MTX and Caco-2 NOD2^{1007fs}/HT29-MTX cells, which remained close to 100% whatever the particle concentrations and size (Figure 7A-D). Then, the impact of these particles on the intestinal barrier integrity was assessed by measuring the TEER and the transepithelial passage of fluorescein, which is a high molecular weight fluorescent dye that crosses the epithelial barrier via the paracellular spaces only if tight junctions are compromised. PCL particles did not alter the integrity of the epithelial barrier, with TEER remaining unchanged, whereas EDTA, used as a positive control, significantly reduced it (Figure 7E-F). It was confirmed by the absence of

fluorescein passage after exposure to pristine or aged PCL particles, unlike the positive control, EDTA (Figure 7G-H).

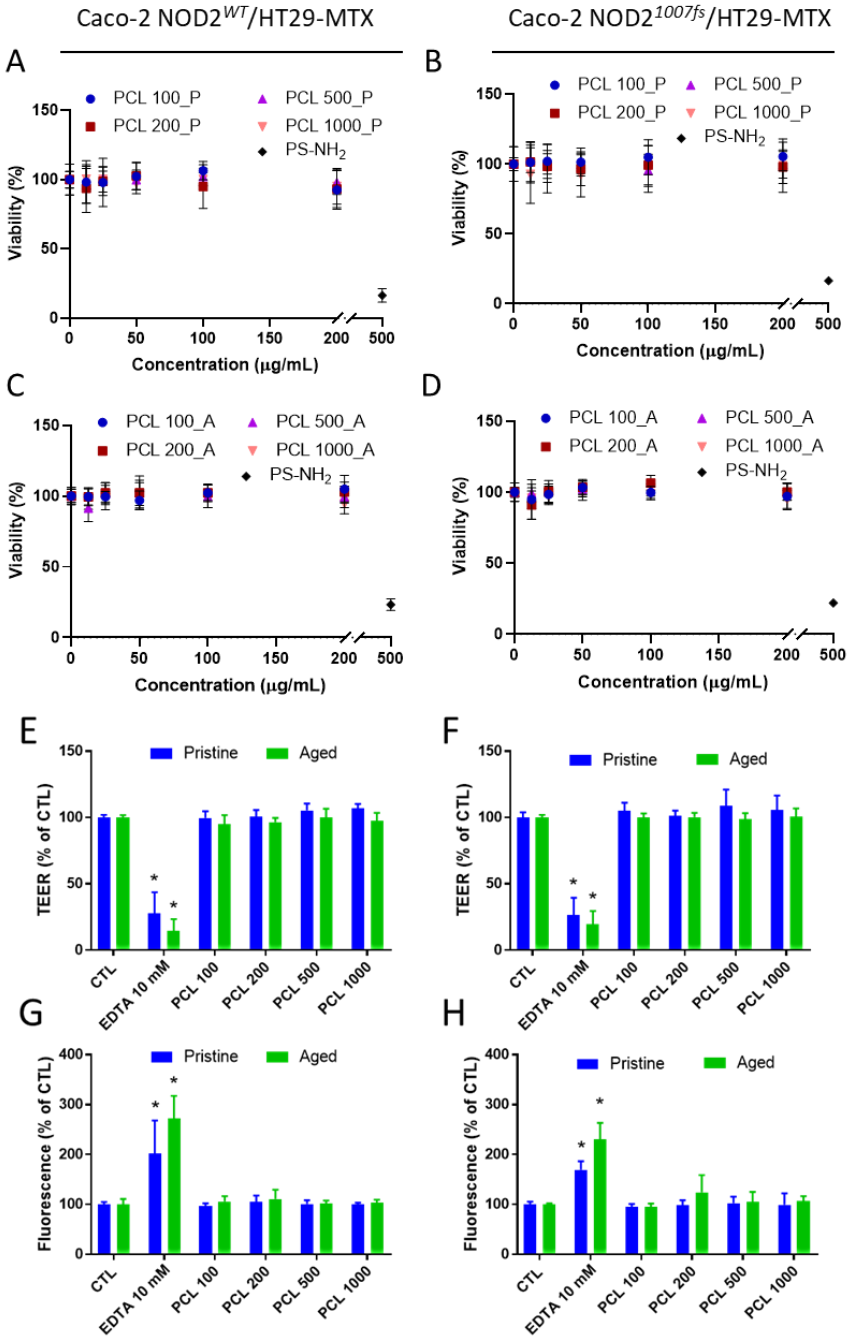

Figure 7. Impact of PCL particles on cell viability and intestinal barrier integrity, in differentiated Caco-2 / HT29-MTX cells. Cells were grown post-confluence for 21 days, then exposed for 24 h to PCL NPLs. Cytotoxicity, as assessed using the WST-1 assay (A-D), after exposure to pristine (PCL_P, A, B) or aged (PCL_A, C, D) PCL NPLs, of Caco-2 NOD2^{WT}/HT29-MTX (A, C) and Caco-2 NOD2^{1007fs}/HT29-MTX (B, D). TEER measurement (E-F) and fluorescein paracellular passage (G-H) through Caco-2 NOD2^{WT}/HT29-MTX (E, G) and Caco-2 NOD2^{1007fs}/HT29-MTX (F, H), exposed to 50 µg/mL pristine (blue) and aged (green) PCL NPLs. PS-NH_2 50 nm particles (500 µg/mL) and EDTA (10 mM) were used as positive controls for the WST-1 and

TEER/fluorescein permeability assays, respectively. Mean ± standard deviation; statistical significance: *p<0.05, exposed vs CTL.

None of the PCL particles investigated, whether pristine or aged, and regardless of their size, induced any increase in intracellular ROS levels after 24 h of exposure compared to the control, neither in Caco-2 NOD2^{WT}/HT29-MTX (Figure 8A) for the 24 h time-point and Figure S8 for all other tested time-points) nor in Caco-2 NOD2^{1007fs}/HT29-MTX cells (Figure 8B for the 24 h time-point and Figure S8 for all other tested time-points), except aged 1000 nm PCL that caused a small but significant decrease of ROS levels. This decrease was small (~10%), which questions its physiological relevance. Neither did PCL particles, either pristine or aged, induce any DNA strand breaks as assessed via the comet assay in alkaline conditions, whatever their size and the cell model (Figure 8C-D and Figure S9).

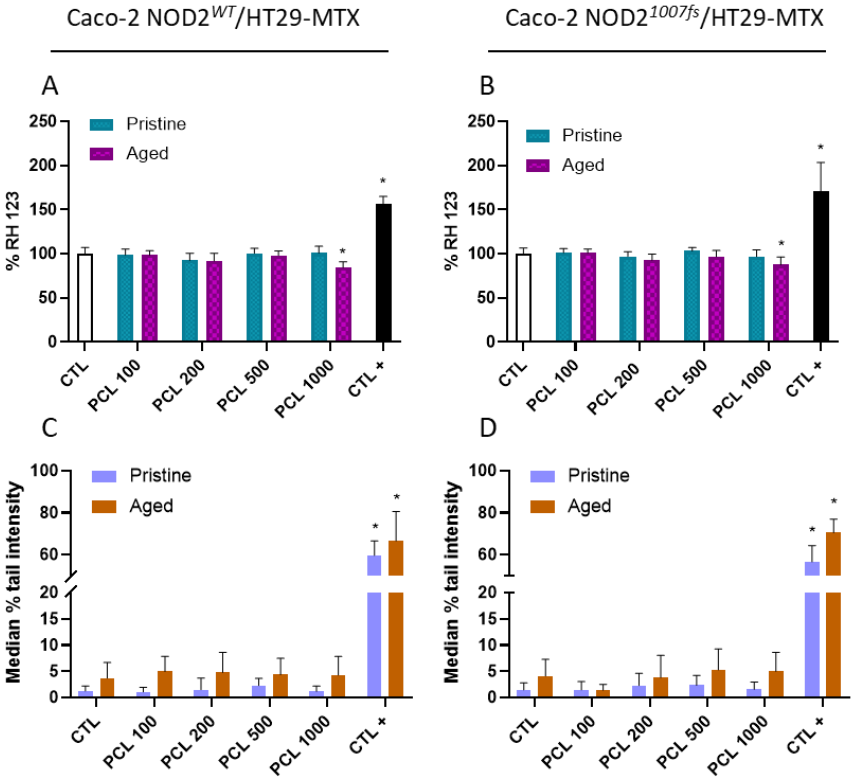

Figure 8. Impact of PCL particles on intracellular ROS levels and DNA integrity in differentiated Caco-2 / HT29-MTX cells. Cells were grown for 21 days post-confluence, then exposed for 24 h to 50 µg/mL PCL NPLs. Intracellular ROS levels (A-B) and DNA strand breaks (C-D) triggered by pristine and aged PCL NPLs with primary diameters 100 nm (PCL 100), 200 nm (PCL 200), 500 nm (PCL 500) or 1000 nm (PCL 1000). Tert-butyl hydroperoxide (1 mM) and methyl methanesulfonate (30 µg/mL) were used as positive controls for the DHR123 and comet assay, respectively. Mean ± standard deviation; statistical significance: *p<0.05, exposed vs CTL.

4. Discussion

Biodegradable plastics, such as PCL, have been developed to improve waste management and they find applications in packaging, 3D printing, and in the medical sector due to their attractive properties [52]. Although PCL is FDA-approved for its biocompatibility, its slow degradation in the body raises concerns about the potential release of MNPs and oligomers that could affect health. Some studies highlighted that PCL are cytotoxic and/or dysregulate immune cell inflammatory response [28-30]. Unlike most studies evaluating the impact of only pristine particles, which are not representative of real-world conditions, this study assessed PCL particles in their pristine state, as well as after artificial aging in a UV test chamber, mimicking sunlight and temperature on a sunny day at noon in the equatorial region [32]. The physicochemical changes induced by particle weathering should be considered in toxicological studies since nanoparticle toxicity mechanisms are closely linked to their physical and chemical properties [31]. We selected particles with sizes ranging from 100 to 1000 nm, as the toxicity of particles made from other polymers, such as polystyrene, is known to be size-dependent [21, 53, 54].

As expected, weathering only slightly affected the shape, size, and surface charge of PCL particles, with significant primary diameter changes restricted to the 100 nm (increase) and 500 nm (decrease) fractions, and a slight shift toward more negative zeta potentials that did not reach statistical significance. However, we previously reported that the same weathering conditions promoted the release of soluble PCL oligomers of varying sizes, from the monomer to the pentamer, thus confirming the sensitivity of this polyester to hydrolysis [33, 34]. Moreover, Raman spectroscopy revealed an increase in the crystallinity of the 200 nm particles after aging, with an intensification of crystalline peaks [55, 56]. This variation could result either from polymer annealing, favouring chain reorganization, or from the degradation of amorphous regions by hydrolysis, leaving only the crystalline areas. The latter hypothesis is supported by several studies that have observed increased PCL crystallinity after chemical or enzymatic hydrolysis [57-60].

PCL toxicity was assessed on *in vitro* cell models based on Caco-2 cells, which is commonly used in intestinal toxicology [61, 62]. These cells were genetically engineered by introduction of NOD2 variants to be representative of healthy individuals (Caco-2 NOD2^{WT}) and of more sensitive individuals, i.e., people showing genetic susceptibility to develop CD (Caco-2 NOD2^{1007fs}), for which some environmental risk factors have been described and among them exposure to particulate matter [63]. We hypothesized that plastic particles could contribute to the development or exacerbation of this disease. This hypothesis is supported by the work of Yan et al., who found a positive correlation between the concentration of MNPs in faeces and the severity of IBD [15], as well as by other research

showing an exacerbation of symptoms in mice with colitis after exposure to MNPs [24, 25]. To enhance the biological relevance of the model, Caco-2 cells were co-cultured with HT29-MTX cells, which secrete some mucus. The study explored the effect of particles on co-cultures at different stages of differentiation, thereby modelling their impact on non-differentiated intestinal epithelium, similar to cells located in intestinal crypts, and differentiated epithelium, characterized by tight junctions and mucus production.

We demonstrated the accumulation of PCL particles in cells, probably by endocytosis in agreement with studies showing the internalization of PS particles with similar size and surface charge in Caco-2 cells [61, 64]. These results are also consistent with other studies reporting the uptake of PCL MNPs by various cell types [28-30]. An interesting consequence of PCL particle internalization is the presence of oligomers in the intracellular compartment. These oligomers could result from particle degradation or from the internalization of oligomers that had formed during the exposure time in the exposure medium, as we previously demonstrated that PCL particles degraded in cell culture medium due to the presence of foetal bovine serum [33]. If oligomers detected in the cell extracts were arising from the internalization of hydrolysis products produced within the exposure medium, the yield of particle degradation in the exposure medium would have to be around 5 % at 24h, which is more than twice the yield that we previously observed, i.e., lower than 2% at 96h [33]. Moreover, the proportion of monomers observed in cells exposed to PCL particles was 24% and 35% after 24h and 48 h, respectively, while in cells exposed to oPCL it was 3 to 4 times higher, with 92% and 98% at 24 h and 48 h, respectively. Therefore, this rules out a major contribution of internalization of oligomers produced within the culture medium and rather suggests that these oligomers originate from PCL particle degradation inside cells. An interesting feature of the detected hydrolysis products is the predominance of short-size oligomers, with the monomer being the major species. This contrasts with results obtained upon aging in water where the pentamer and tetramer were the most frequent products. These observations suggest that esterases and lipases produced by Caco-2 cells are actively involved in the intracellular hydrolysis of PCL [65-69].

It is essential to evaluate the toxicity of the released oligomers, which may differ from that of the intact particles, as has been observed with other plastics, including PS, PC and PVC, containing toxic monomers with detrimental effects on human health [70]. Although our results confirm the accumulation of PCL particles in cells and their degradation into oligomers, no toxicity was observed, whatever the particle size, in terms of cell viability, ROS production, epithelial barrier integrity, DNA integrity, or IL-8 secretion. Synthetic oligomers did not cause any cytotoxicity as well. These findings hold true regardless of cell differentiation or genetic susceptibility to CD. However, some alterations in mRNA expression were observed, proving that cells responded to PCL particle exposure, although

in a homeostatic manner. Indeed, exposure to PCL particles induced endoplasmic reticulum stress response, leading to the modulation of unfolded protein response markers, as previously demonstrated in mice exposed to PS particles [71]. Disruption of protein folding can compromise cellular homeostasis and, if adaptive mechanisms fail, it would trigger apoptosis [72]. In cells expressing wild-type NOD2, ATF6 was induced, while cells expressing NOD2^{1007fs} exhibited overexpression of GRP78 and sXBP1, suggesting a link to CD. Indeed, elevated levels of GRP78 and sXBP1 have been detected in the inflamed intestines of patients with CD, suggesting that ER stress promotes chronic inflammation [73]. Moreover, significant changes in endoplasmic reticulum proteins levels have also been reported in macrophages exposed to 200 nm PCL particles [28]. We also observed that exposure to PCL particles altered the expression of ABC transporters, notably MDR1 (i.e., the P-gp) and MRP1, in line with studies showing that other particle internalization can impact these transporters [53, 74]. ABC transporters play key roles in the efflux of xenobiotics and in cellular protection [75]. Still, these alterations should be confirmed at the protein level (e.g., by Western blot or proteomics) or at the functional level, and ideally validated in more physiologically relevant models, such as primary cells or organoid models.

To our knowledge, no study has yet examined the effects of PCL NPLs on Caco-2/HT29-MTX intestinal cells. However, our observations are consistent with studies conducted on other NPLs, such as PS, PP, and PA, which report little to no toxic effects on these human intestinal cells, regardless of their level of differentiation [53, 61, 64, 76-78]. Similarly, recent studies conducted in our laboratory showed that PS-COOH, PET and PLA NPLs do not induce any toxic effects on the same intestinal models as those used in this study [44, 45]. However, it is important to note that the effects of NPLs vary considerably between *in vitro* and *in vivo* studies. Research has shown that various NPLs (PS, PE, PP, PA, and PVC) cause significant intestinal effects in the zebrafish, *C. elegans*, and mice [17-19, 79, 80]. For example, Jin et al. showed that exposure to PS NPLs caused dysbiosis, intestinal barrier dysfunction, and metabolic disorders in mice [20]. Similarly, Dussol et al. observed increased sensitivity to PS-COOH NPLs in *Nod2*^{KO} mice compared to *Nod2*^{WT} mice, while no impact was observed on Caco-2 (NOD2^{WT} or NOD2^{1007fs}) / HT29-MTX *in vitro* models [45]. These results suggest that individuals with genetic susceptibility to CD may be more affected by exposure to NPLs than healthy individuals. They highlight the lower sensitivity of Caco-2/HT29-MTX co-cultures compared to *in vivo* mouse models [45]. An important caveat of these epithelial models is the use of Caco-2 and HT29-MTX cancer-derived cell lines, which may not fully reproduce the phenotype, differentiation state, barrier physiology and stress responses of primary intestinal epithelium, especially when considering their genotype, which is not normal. The properties of mucus produced by HT29-MTX remain an approximation of physiological intestinal mucus [81, 82]. Moreover, it would be more suitable to evaluate ER stress on cells that would

produce and manufacture large amounts of proteins such as Goblet cells or Paneth cells, instead of epithelial cells [83]. Beyond these cell line-related considerations, such *in vitro* models lack representativeness of the intestine, particularly because they do not include any immune cells and microbiota. The latter is a drastic difference between *in vitro* and *in vivo* models. Indeed, the microbiota plays a crucial role in intestinal homeostasis and is influenced by various environmental factors, such as diet and medication [84]. Many *in vivo* studies have shown that exposure to NPLs causes intestinal disturbances, including dysbiosis [18, 85]. This imbalance can impair the intestinal barrier, promote chronic inflammation, and contribute to the development of diseases such as IBD [86]. A recent study showed that PS NPLs induce dysbiosis, oxidative stress, intestinal damage, and systemic inflammation in mice. These effects were significantly attenuated in microbiota-depleted mice, suggesting that the microbiota may mediate the toxicity of PS NPLs on the intestine [21]. These results align with the work of Qiao et al., who highlighted a major indirect impact of dysbiosis in the intestinal barrier dysfunction induced by PS NPLs in mice, thereby emphasizing the central role of the microbiota in the toxicity of NPLs [87]. Finally, the model does not include digestion simulation, where pH variations and other physicochemical conditions may alter particle properties and their interactions with the epithelium [88, 89].

Thus, to overcome these limitations, it would be relevant to integrate the microbiota as well as immune cells, which are essential for studying the symptoms of IBD, and to pre-condition particles by passing them through simulated digestive fluids to better reproduce gastrointestinal tract conditions. The development of more complex intestinal models, such as organoids or primary cells, would allow for the *in vitro* reproduction of an environment closer to the *in vivo* intestine [90]. The use of models combining human intestinal epithelial cells, immune cells, and the microbiota, for example on microfluidic chips, would be a promising approach to assess the effects of plastic NPLs on the intestine [91]. Beyond improving the physiological relevance of the model, refining the exposure design is also important to better capture response dynamics. Most endpoints were assessed after a single 24 h exposure, although intracellular accumulation was observed. For potentially accumulating materials, a 24 h exposure may be insufficient to rule out transient, delayed, or cumulative responses; therefore, the present data primarily support conclusions on acute effects. Future work would benefit from incorporating kinetic measurements (e.g., 0, 6, 12, 24, 48, and 72 h) and/or longer or repeated exposure regimens (e.g., daily re-dosing with media renewal over several days) to better capture accumulation-driven responses.

Another outcome of this work is that aging particles did not increase their toxicity on intestinal models, which is often reported in the literature. For example, a study on PS particles, either pristine or aged by UV irradiation, highlighted a higher cytotoxicity of the oxidized particles on Caco-2 cells [92].

Similarly, PCL particles aged by alkaline treatment (NaOH), inducing hydrolysis and generating reactive groups (carboxyl and hydroxyl), caused increased toxicity, in terms of cell viability and reduced hemocompatibility [29]. Furthermore, PCL oligomers did not show cytotoxicity, which is consistent with a study indicating low toxicity of 6-hydroxyhexanoic acid on fibroblasts [93], but contrasts with another study showing that PLA oligomers caused intestinal damage and acute inflammation in mice [94]. However, in this latter case, the final degradation product of PLA oligomers is lactic acid. Excess of this glycolysis end by-product may thus perturb metabolic networks more than longer hydroxy acids such as 6-hydroxyhexanoic acid. Comparing these studies is complex due to the diversity of aging protocols, the types of NPLs and oligomers analysed, the characterization methods, and the models and toxicity tests employed. This heterogeneity makes the assessment of NPLs' hazard challenging. Therefore, it is crucial to standardize NPLs toxicity studies to ensure reliable and scientifically sound conclusions, as recommended by several authors [32, 95].

5. Conclusion

This study assessed the toxic effects of PCL NPLs on human colon epithelium models, in vitro, taking into account their aging in conditions mimicking a journey in the environment. Our results show that aging modifies the physicochemical properties of the particles, leading to increased crystallinity and the release of oligomers through hydrolysis. Both pristine and aged PCL NPLs did not trigger any toxicity in the assessed exposure conditions, regardless of particle size, their pristine or aged state, or cell phenotype. PCL NPLs accumulated in these cells without affecting their viability, ROS production, DNA integrity, epithelial barrier integrity or IL-8 secretion. However, changes in the expression of some endoplasmic reticulum stress markers and ABC transporters were detected, suggesting subtle responses to PCL NPL exposure. These results align with studies on other NPLs, showing low toxicity, *in vitro*, upon acute exposure. However, the limitations of the models used, particularly the absence of microbiota and immune cells, and the focus on colon cells only, highlight the need for more complex systems to better understand the effects of NPLs on the intestine. Finally, the heterogeneity of experimental protocols emphasizes the importance of standardizing studies to better understand the impact of MNPs on human health.

6. Acknowledgements

This project received help from the CEA flow cytometry facility, which is funded by GRAL, a programme from the Chemistry Biology Health Graduate School of University Grenoble Alpes (ANR-

17-EURE-0003). It used the electron microscopy facility at the Grenoble Instruct-ERIC Center (ISBG; UAR 3518 CNRS CEA-UGA-EMBL) with support from the French Infrastructure for Integrated Structural Biology (FRISBI; ANR-10-INSB-05-02) and GRAL, a project of the University Grenoble Alpes graduate school (Ecoles Universitaires de Recherche) CBHEUR-GS (ANR-17-EURE-0003). The IBS Electron Microscope facility is supported by the Auvergne Rhône-Alpes Région, the Fonds Feder, the Fondation pour la Recherche Médicale and GIS-IBiSA. It was operated by Daphna Fenel and Emma Dusacq, and Guy Schoen is kindly acknowledged for its participation in the EM facility maintenance.

7. Funding

This work was conducted in the frame of the PLASTOX project, which received funding from the Agence Nationale de la Recherche (ANR, PLASTOX grant ANR-21-CE34-0028-02), the Agence Nationale de Sécurité Environnementale et Sanitaire (ANSES, EXMINA grant, PNR EST-21-077) and by the European Union's Horizon 2020 research and innovation programme under grant agreement no. 965196 (PLASTICHEAL). This project was financially supported by the French government through the France 2030 investment plan managed by the French National Research Agency (ANR, PEPR Recyclage, ANR-22-PERE-0007).

8. Conflict of interest

The authors declare no conflict of interest

9. Authors contribution

Investigation: MB, VB, MP, DB, SD, DF, ED, VCF, TR, TD; Formal analysis: MB, VB, MP, SD, VCF, TD. Conceptualization, Methodology, Validation, Supervision: MC, TD; Visualization: MB, VB, MP, DB, DF, CM, TD, MC; Funding acquisition, Resources, Project administration: MC; Writing-original draft: MB, MC, Writing-review and editing: MB, TR, TD, MC.

10. References

1. Andrady, A. and M. Neal, *Applications and societal benefits of plastics.* Philosophical Transactions of the Royal Society B-Biological Sciences, 2009. **364**(1526): p. 1977–1984.
2. Geyer, R., J. Jambeck, and K. Law, *Production, use, and fate of all plastics ever made.* Science Advances, 2017. **3**(7).
3. Lau, W., et al., *Evaluating scenarios toward zero plastic pollution.* Science, 2020. **369**(6510): p. 1455–1461.
4. Jambeck, J.R., et al., *Marine pollution. Plastic waste inputs from land into the ocean.* Science, 2015. **347**(6223): p. 768–71.
5. Zhang, K., et al., *Understanding plastic degradation and microplastic formation in the environment: A review.* Environmental Pollution, 2021. **274**.
6. EFSA panel on contaminants in the food chain (CONTAM), *Presence of microplastics and nanoplastics in food, with particular focus on seafood.* EFSA Journal, 2016. **14**(6): p. 4501.
7. Hartmann, N., et al., *Are We Speaking the Same Language? Recommendations for a Definition and Categorization Framework for Plastic Debris.* Environmental Science & Technology, 2019. **53**(3): p. 1039–1047.
8. Galloway, T., *Micro-and Nano-plastics and Human Health*, in *Marine Anthropogenic Litter*. 2015. p. 343–366.
9. Schymanski, D., et al., *Analysis of microplastics in water by micro-Raman spectroscopy: Release of plastic particles from different packaging into mineral water.* Water Research, 2018. **129**: p. 154–162.
10. Toussaint, B., et al., *Review of micro- and nanoplastic contamination in the food chain.* Food Additives and Contaminants Part a-Chemistry Analysis Control Exposure & Risk Assessment, 2019. **36**(5): p. 639–673.
11. Kosuth, M., S. Mason, and E. Wattenberg, *Anthropogenic contamination of tap water, beer, and sea salt.* Plos One, 2018. **13**(4).
12. Senathirajah, K., et al., *Estimation of the mass of microplastics ingested - A pivotal first step towards human health risk assessment.* Journal of Hazardous Materials, 2021. **404**.
13. Ma, C., et al., *Application of internal persistent fluorescent fibers in tracking microplastics in vivo processes in aquatic organisms.* J Hazard Mater, 2021. **401**: p. 123336.
14. Schwabl, P., et al., *Detection of Various Microplastics in Human Stool A Prospective Case Series.* Annals of Internal Medicine, 2019. **171**(7): p. 453–457.
15. Yan, Z., et al., *Analysis of Microplastics in Human Feces Reveals a Correlation between Fecal Microplastics and Inflammatory Bowel Disease Status.* Environmental Science & Technology, 2022. **56**(1): p. 414–421.
16. Zhang, J., et al., *Occurrence of Polyethylene Terephthalate and Polycarbonate Microplastics in Infant and Adult Feces.* Environmental Science & Technology Letters, 2021. **8**(11): p. 989–994.
17. Li, Y., et al., *Microplastics in the human body: A comprehensive review of exposure, distribution, migration mechanisms, and toxicity.* Sci Total Environ, 2024. **946**: p. 174215.
18. Qiao, R., et al., *Accumulation of different shapes of microplastics initiates intestinal injury and gut microbiota dysbiosis in the gut of zebrafish.* Chemosphere, 2019. **236**.
19. Deng, Y., et al., *Tissue accumulation of microplastics in mice and biomarker responses suggest widespread health risks of exposure.* Scientific Reports, 2017. **7**.
20. Jin, Y., et al., *Impacts of polystyrene microplastic on the gut barrier, microbiota and metabolism of mice.* Science of the Total Environment, 2019. **649**: p. 308–317.
21. Lin, H., et al., *The role of gut microbiota in mediating increased toxicity of nano-sized polystyrene compared to micro-sized polystyrene in mice.* Chemosphere, 2024. **358**: p. 142275.
22. Jones, L.R., S.J. Wright, and T.W. Gant, *A critical review of microplastics toxicity and potential adverse outcome pathway in human gastrointestinal tract following oral exposure.* Toxicology Letters, 2023. **385**: p. 51–60.

23. Torres, J., et al., *Crohn's disease.* Lancet, 2017. **389**(10080): p. 1741–1755.
24. Luo, T., et al., *Polystyrene microplastics exacerbate experimental colitis in mice tightly associated with the occurrence of hepatic inflammation.* Science of the Total Environment, 2022. **844**.
25. Zheng, H., et al., *Proinflammatory properties and lipid disturbance of polystyrene microplastics in the livers of mice with acute colitis.* Science of the Total Environment, 2021. **750**.
26. Napper, I. and R. Thompson, *Environmental Deterioration of Biodegradable, Oxo-biodegradable, Compostable, and Conventional Plastic Carrier Bags in the Sea, Soil, and Open-Air Over a 3-Year Period.* Environmental Science & Technology, 2019. **53**(9): p. 4775–4783.
27. Ntrivala, M.A., et al., *Polycaprolactone (PCL): the biodegradable polyester shaping the future of materials – a review on synthesis, properties, biodegradation, applications and future perspectives.* European Polymer Journal, 2025. **234**: p. 114033.
28. Collin-Faure, V., et al., *A comparison of the effects of polystyrene and polycaprolactone nanoplastics on macrophages.* Environmental Science-Nano, 2025. **12**(8): p. 3990–4007.
29. Jesus, S., et al., *Unravelling the Immunotoxicity of Polycaprolactone Nanoparticles-Effects of Polymer Molecular Weight, Hydrolysis, and Blends.* Chemical Research in Toxicology, 2020. **33**(11): p. 2819–2833.
30. Singh, R. and P. Ramarao, *Accumulated Polymer Degradation Products as Effector Molecules in Cytotoxicity of Polymeric Nanoparticles.* Toxicological Sciences, 2013. **136**(1): p. 131–143.
31. Sukhanova, A., et al., *Dependence of Nanoparticle Toxicity on Their Physical and Chemical Properties.* Nanoscale Research Letters, 2018. **13**.
32. Waldman, W. and M. Rillig, *Microplastic Research Should Embrace the Complexity of Secondary Particles.* Environmental Science & Technology, 2020. **54**(13): p. 7751–7753.
33. Boulée, M., M. Carrière, and T. Douki, *Quantitative HPLC–mass spectrometry analysis shows the drastic impact of the composition of aqueous and biochemical media on the release of soluble hydrolysis products from submicron polycaprolactone.* Polymer, 2025. **339**: p. 129150.
34. Douki, T., et al., *Extensive HPLC-tandem mass spectrometry characterization of soluble degradation products of biodegradable nanoplastics under environmentally relevant temperature and irradiation conditions.* Environmental Science-Nano, 2024. **11**(9): p. 3956–3965.
35. Leonard, F., E. Collnot, and C. Lehr, *A Three-Dimensional Coculture of Enterocytes, Monocytes and Dendritic Cells To Model Inflamed Intestinal Mucosa in Vitro.* Molecular Pharmaceutics, 2010. **7**(6): p. 2103–2119.
36. Girardin, S., et al., *Nod2 is a general sensor of peptidoglycan through muramyl dipeptide (MDP) detection.* Journal of Biological Chemistry, 2003. **278**(11): p. 8869–8872.
37. Economou, M., et al., *Differential effects of NOD2 variants on Crohn's disease risk and phenotype in diverse populations: A metaanalysis.* American Journal of Gastroenterology, 2004. **99**(12): p. 2393–2404.
38. Schnitzler, F., et al., *The NOD2 p.Leu1007fsX1008 Mutation (rs2066847) Is a Stronger Predictor of the Clinical Course of Crohn's Disease than the FOXO3A Intron Variant rs12212067.* Plos One, 2014. **9**(11).
39. Inohara, N., et al., *Host recognition of bacterial muramyl dipeptide mediated through NOD2.* Journal of Biological Chemistry, 2003. **278**(8): p. 5509–5512.
40. Lesuffleur, T., et al., *Growth adaptation to methothrexate of HT-29 human colon-carcinoma cells is associated with their ability to differentiate into columnar absorptive and mucus-secreting cells.* Cancer Research, 1990. **50**(19): p. 6334–6343.
41. Dorier, M., et al., *The food additive E171 and titanium dioxide nanoparticles indirectly alter the homeostasis of human intestinal epithelial cells in vitro.* Environmental Science-Nano, 2019. **6**(5): p. 1549–1561.
42. Behnke, T., et al., *Encapsulation of Hydrophobic Dyes in Polystyrene Micro- and Nanoparticles via Swelling Procedures.* Journal of Fluorescence, 2011. **21**(3): p. 937–944.

43. Li, M., et al., *Easy preparation and characterization of highly fluorescent polymer composite microspheres from aqueous CdTe nanocrystals.* Journal of Colloid and Interface Science, 2006. **300**(2): p. 564–568.
44. Bard, V.B., M.; Villacorta, A.; Fenel, D.; Moriscot, C.; Marcos, R.; Hernández, A.; Douki, T.; Carrière, M, *PET and PLA Particles Accumulate in Human Intestinal Epithelium Representative of Healthy Individuals and Patients with Crohn's Disease, in Vitro, but Do Not Cause Significant Toxicity.* unpublished data.
45. Dussol, M.M., S; Boulee, M; Bard, V; Airaud, M; Fenel, D; Moriscot, C; Barreau, F; Carriere, M, *Toxicity of polystyrene particles to mice and in vitro models of intestinal cells, both healthy 1 and with genetic susceptibility to Crohn's disease.* unpublished data.
46. Lesuffleur, T., et al., *Growth adaptation to methothrexate f HT-29 human colon-carcinoma cells is associated with their ability to differentiate into columnar absorptive and mucus-secreting cells.* Cancer Research, 1990. **50**(19): p. 6334–6343.
47. Senathirajah, K., et al., *Estimation of the mass of microplastics ingested - A pivotal first step towards human health risk assessment.* J Hazard Mater, 2021. **404**(Pt B): p. 124004.
48. Helander, H.F. and L. Fändriks, *Surface area of the digestive tract – revisited.* Scandinavian Journal of Gastroenterology, 2014. **49**(6): p. 681–689.
49. Ude, V., et al., *Impact of copper oxide nanomaterials on differentiated and undifferentiated Caco-2 intestinal epithelial cells; assessment of cytotoxicity, barrier integrity, cytokine production and nanomaterial penetration.* Particle and Fibre Toxicology, 2017. **14**.
50. Bessa, M.J., et al., *Optimization of the harvesting and freezing conditions of human cell lines for DNA damage analysis by the alkaline comet assay.* Mutation Research/Genetic Toxicology and Environmental Mutagenesis, 2019. **845**: p. 402994.
51. Pfaffl, M.W., G.W. Horgan, and L. Dempfle, *Relative expression software tool (REST) for group-wise comparison and statistical analysis of relative expression results in real-time PCR.* Nucleic Acids Res, 2002. **30**(9): p. e36.
52. Woodruff, M.A. and D.W. Hutmacher, *The return of a forgotten polymer—Polycaprolactone in the 21st century.* Progress in Polymer Science, 2010. **35**(10): p. 1217–1256.
53. Wu, B., et al., *Size-dependent effects of polystyrene microplastics on cytotoxicity and efflux pump inhibition in human Caco-2 cells.* Chemosphere, 2019. **221**: p. 333–341.
54. Shang, L., K. Nienhaus, and G.U. Nienhaus, *Engineered nanoparticles interacting with cells: size matters.* J Nanobiotechnology, 2014. **12**: p. 5.
55. Kister, G., et al., *Structural characterization and hydrolytic degradation of solid copolymers of D,L-lactide-co-ε-caprolactone by Raman spectroscopy.* Polymer, 2000. **41**(3): p. 925–932.
56. Taddei, P., et al., *In vitro bioactivity of poly(ε-caprolactone)-apatite (PCL-AP) scaffolds for bone tissue engineering:: The influence of the PCL/AP ratio.* International Journal of Artificial Organs, 2006. **29**(7): p. 719–725.
57. Ali, S., et al., *Mechanisms of polymer degradation in implantable devices. 1. Poly(caprolactone).* Biomaterials, 1993. **14**(9): p. 648–656.
58. Castilla-Cortázar, I., et al., *Hydrolytic and enzymatic degradation of a poly(ε-caprolactone) network.* Polymer Degradation and Stability, 2012. **97**(8): p. 1241–1248.
59. Dias, J., et al., *Electrospun Polycaprolactone (PCL) Degradation: An In Vitro and In Vivo Study.* Polymers, 2022. **14**(16).
60. Taddei, P., A. Tinti, and G. Fini, *Vibrational spectroscopy of polymeric biomaterials.* Journal of Raman Spectroscopy, 2001. **32**(8): p. 619–629.
61. Domenech, J., et al., *Long-Term Effects of Polystyrene Nanoplastics in Human Intestinal Caco-2 Cells.* Biomolecules, 2021. **11**(10).
62. Guibourdenche, M., et al., *Food Contaminants Effects on an In Vitro Model of Human Intestinal Epithelium.* Toxics, 2021. **9**(6).
63. Nishida, A., et al., *Gut microbiota in the pathogenesis of inflammatory bowel disease.* Clin J Gastroenterol, 2018. **11**(1): p. 1–10.

64. Cortés, C., et al., *Nanoplastics as a potential environmental health factor: effects of polystyrene nanoparticles on human intestinal epithelial Caco-2 cells.* Environmental Science-Nano, 2020. **7**(1): p. 272–285.
65. Bartnikowski, M., et al., *Degradation mechanisms of polycaprolactone in the context of chemistry, geometry and environment.* Progress in Polymer Science, 2019. **96**: p. 1–20.
66. Chang, H., et al., *In vivo degradation of poly (ε-caprolactone) films in Gastro Intestinal (GI) tract.* Materials Today Communications, 2017. **11**: p. 18–25.
67. Imai, T., et al., *Identification of esterases expressed in Caco-2 cells and effects of their hydrolyzing activity in predicting human intestinal absorption.* Drug Metabolism and Disposition, 2005. **33**(8): p. 1185–1190.
68. Li, S., et al., *Lipase-catalyzed biodegradation of poly(ε-caprolactone) blended with various polylactide-based polymers.* Biomacromolecules, 2003. **4**(2): p. 372–377.
69. Spalinger, J., et al., *Endogenous lipase activity in Caco-2 cells.* Biochimica Et Biophysica Acta-Lipids and Lipid Metabolism, 1998. **1393**(1): p. 119–127.
70. Lithner, D., Å. Larsson, and G. Dave, *Environmental and health hazard ranking and assessment of plastic polymers based on chemical composition.* Science of the Total Environment, 2011. **409**(18): p. 3309–3324.
71. Chen, Y., et al., *Acute exposure to polystyrene nanoplastics induces unfolded protein response and global protein ubiquitination in lungs of mice.* Ecotoxicology and Environmental Safety, 2024. **280**.
72. Chakrabarti, A., A. Chen, and J. Varner, *A Review of the Mammalian Unfolded Protein Response.* Biotechnology and Bioengineering, 2011. **108**(12): p. 2777–2793.
73. Solà Tapias, N., et al., *Colitis Linked to Endoplasmic Reticulum Stress Induces Trypsin Activity Affecting Epithelial Functions.* J Crohns Colitis, 2021. **15**(9): p. 1528–1541.
74. Yu, J., et al., *Comparison of Cytotoxicity and Inhibition of Membrane ABC Transporters Induced by MWCNTs with Different Length and Functional Groups.* Environmental Science & Technology, 2016. **50**(7): p. 3985–3994.
75. Pohl, P., et al., *ABC transporter efflux pumps: A defense mechanism against ivermectin in Rhipicephalus (Boophilus) microplus.* International Journal for Parasitology, 2011. **41**(13-14): p. 1323–1333.
76. Busch, M., et al., *Investigations of acute effects of polystyrene and polyvinyl chloride micro- and nanoplastics in an advanced in vitro triple culture model of the healthy and inflamed intestine.* Environmental Research, 2021. **193**.
77. Domenech, J., et al., *Interactions of polystyrene nanoplastics with in vitro models of the human intestinal barrier.* Archives of Toxicology, 2020. **94**(9): p. 2997–3012.
78. Lehner, R., et al., *A novel 3D intestine barrier model to study the immune response upon exposure to microplastics.* Archives of Toxicology, 2020. **94**(7): p. 2463–2479.
79. Jia, R., et al., *Exposure to Polypropylene Microplastics via Oral Ingestion Induces Colonic Apoptosis and Intestinal Barrier Damage through Oxidative Stress and Inflammation in Mice.* Toxics, 2023. **11**(2).
80. Lei, L., et al., *Microplastic particles cause intestinal damage and other adverse effects in zebrafish Danio rerio and nematode Caenorhabditis elegans.* Science of the Total Environment, 2018. **619**: p. 1–8.
81. Fedi, A., et al., *In vitro models replicating the human intestinal epithelium for absorption and metabolism studies: A systematic review.* Journal of Controlled Release, 2021. **335**: p. 247–268.
82. Lopez-Escalera, S. and A. Wellejus, *Evaluation of Caco-2 and human intestinal epithelial cells as in vitro models of colonic and small intestinal integrity.* Biochem Biophys Rep, 2022. **31**: p. 101314.
83. McGuckin, M.A., et al., *ER stress and the unfolded protein response in intestinal inflammation.* American Journal of Physiology-Gastrointestinal and Liver Physiology, 2010. **298**(6): p. G820–G832.

84. Natividad, J. and E. Verdu, *Modulation of intestinal barrier by intestinal microbiota: Pathological and therapeutic implications.* Pharmacological Research, 2013. **69**(1): p. 42–51.
85. Chen, X., et al., *Polyvinyl chloride microplastics induced gut barrier dysfunction, microbiota dysbiosis and metabolism disorder in adult mice.* Ecotoxicology and Environmental Safety, 2022. **241**.
86. Cerf-Bensussan, N. and V. Gaboriau-Routhiau, *The immune system and the gut microbiota: friends or foes?* Nat Rev Immunol, 2010. **10**(10): p. 735–44.
87. Qiao, J., et al., *Perturbation of gut microbiota plays an important role in micro/nanoplastics-induced gut barrier dysfunction.* Nanoscale, 2021. **13**(19): p. 8806–8816.
88. Kose, O., et al., *Physicochemical Transformations of Silver Nanoparticles in the Oro-Gastrointestinal Tract Mildly Affect Their Toxicity to Intestinal Cells In Vitro: An AOP-Oriented Testing Approach.* Toxics, 2023. **11**(3): p. 199.
89. Liu, S., et al., *Influence of the digestive process on intestinal toxicity of polystyrene microplastics as determined by in vitro Caco-2 models.* Chemosphere, 2020. **256**: p. 127204.
90. Sato, T., et al., *Single Lgr5 stem cells build crypt-villus structures in vitro without a mesenchymal niche.* Nature, 2009. **459**(7244): p. 262–U147.
91. Bein, A., et al., *Microfluidic Organ-on-a-Chip Models of Human Intestine.* Cellular and Molecular Gastroenterology and Hepatology, 2018. **5**(4): p. 659–668.
92. Yu, X., et al., *Photo-transformation of microplastics and its toxicity to Caco-2 cells.* Science of the Total Environment, 2022. **806**.
93. Orchel, A., et al., *Growth of human fibroblasts in the presence of 6-hydrohexanoic acid.* Acta Poloniae Pharmaceutica, 2010. **67**(6): p. 710–712.
94. Wang, M., et al., *Oligomer nanoparticle release from polylactic acid plastics catalysed by gut enzymes triggers acute inflammation.* Nature Nanotechnology, 2023. **18**(4).
95. Brachner, A., et al., *Assessment of Human Health Risks Posed by Nano-and Microplastics Is Currently Not Feasible.* International Journal of Environmental Research and Public Health, 2020. **17**(23).

Supplementary Materials

Table S2. RT-qPCR primers sequences

	Forward primer (5'> 3')	Reverse primer (5'>3')
Reference genes		
GAPDH	GAGTCAACGGATTTGGTCGT	TTGATTTTGGAGGGATCTCG
CYCLOB	GCAAGATCGAGGTGGAGAAG	CTGTGGAATGTGAGGGGAGT
Oxidative stress		
CAT	AGCTTAGCGTTCATCCGTGT	TCCAATCATCCGTCAAAACA
SOD1	AGGGCATCATCAATTTCGAG	ACATTGCCCAAGTCTCCAAC
SOD2	TCCACTGCAAGGAACAACAG	TCTTGCTGGGATCATTAGGG
GCLM	AGTCCTTGGAGTTGCACAGC	ACACAGCAGGACGCAAGATT
HO-1	TTCTCCGATGGGTCCTTACACT	GGCATAAAGCCCTACAGCAACT
Inflammation		
IL-1β	CTCGCCAGTGAAATGATGGCT	TAGGTCGATGCTTAGAGGCTG
IL-8	TGGCAGCCTTCCTGATTTCT	ATTTCTGTGTTGGCGCAGTG
TNFα	GGCGTGGAGCTGAGAGATAAC	GGTGTGGGTGAGGAGCACAT
Endoplasmic reticulum stress		
GRP78	GGTGAAAGACCCCTGACAAA	GTCAGGCGATTCTGGTCATT
IRE1	AGAGAGGCGGGAGAGCCGTG	CGAGGAGGTGGGGGAAGCGA
CHOP	TGGAAGCCTGGTATGAGGAC	TGTGACCTCTGCTGGTTCTG
sXBP1	GCAGGTGCAGGCCCAGTTGT	TGGGTCCAAGTTGTCCAGAATGC
ATF6	CCAGCAGCACCCAAGACTCAAACA	GTGTGACTCCCCCAGCAACAGC
Mucin		
MUC5AC	TCCACCATATACCGCCACAGA	TGGACGGACAGTCACTGTCAAC
ABC transporters		
MDR1	GCCAAAGCCAAAATATCAGC	TTCCAATGTGTTCGGCAT
MRP1	GGGCTGCGGAAAGTCGT	AGCCCTTGATAGCCACGTG
MRP2	TGAGCAAGTTTGAAACGCACAT	AGCTCTTCTCCTGCCGTCTCT
BCRP	TGCAACATGTACTGGCGAAGA	TCTTCCACAAGCCCCAGG

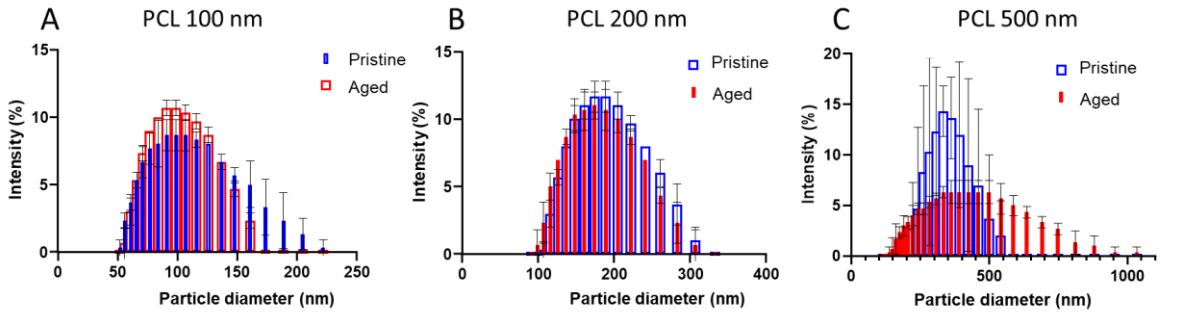

Figure S1. Size distribution of PCL particles. Size distribution histograms of pristine (blue) and aged (red) PCL particles, with primary diameter 100 nm (A), 200 nm (B) and 500 nm (C), as measured by DLS.

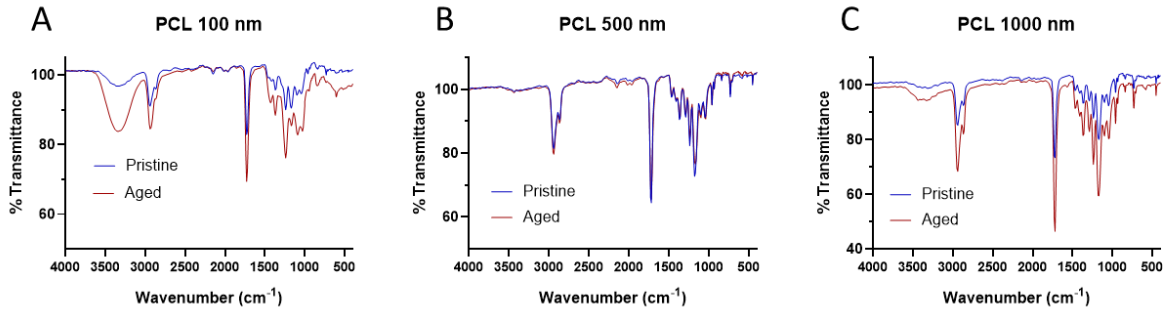

Figure S2. FTIR analysis of PCL particles. FTIR spectra of pristine (blue) and aged (red) PCL particles, with primary diameters 100 nm (A), 500 nm (B) and 1000 nm (C).

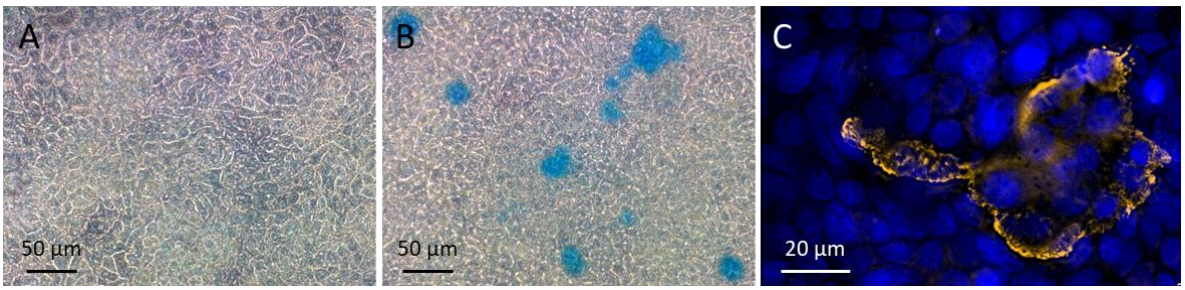

Figure S3. Mucus secretion by Caco-2 NOD2^{1007fs}/HT29-MTX cells. Alcian blue staining of Caco-2 NOD2^{1007fs} monoculture (A) and Caco-2 NOD2^{1007fs}/HT29-MTX co-culture (B). MUC5AC immunostaining of the Caco-2 NOD2^{1007fs}/HT29-MTX co-culture (C).

Table S2. Exposure metrics[a]

Nr. Particle per well

96-well

Pristine	12,5 µg/mL	25 µg/mL	50 µg/mL	100 µg/mL	200 µg/mL
100 nm	$2.9x10^{11}$	$5.9x10^{11}$	$1.2x10^{12}$	$2.4x10^{12}$	$4,7x10^{12}$
200 nm	$4.4x10^{10}$	$8.8x10^{10}$	$1.8x10^{11}$	$3.5x10^{11}$	$7,0x10^{11}$
500 nm	$6.4x10^{9}$	$1.3x10^{10}$	$2.5x10^{10}$	$5.1x10^{10}$	$1,0x10^{11}$
1000 nm	$1.4x10^{10}$	$2.7x10^{10}$	$5.,4x10^{10}$	$1.1x10^{11}$	$2,2x10^{11}$

Aged	12,5 µg/mL	25 µg/mL	50 µg/mL	100 µg/mL	200 µg/mL
100 nm	$3.0x10^{11}$	$5.9x10^{11}$	$1.2x10^{12}$	$2.4x10^{12}$	$4.8x10^{12}$
200 nm	$5.2x10^{10}$	$1.0x10^{11}$	$2.1x10^{11}$	$4.2x10^{11}$	$8.4x10^{11}$
500 nm	$8.6x10^{09}$	$1.7x10^{10}$	$3.5x10^{10}$	$6.9x10^{10}$	$1.4x10^{11}$
1000 nm	$5.0x10^{10}$	$9.9x10^{10}$	$2.0x10^{11}$	$4.0x10^{11}$	$7.9x10^{11}$

12-well

Pristine	50 µg/mL
100 nm	$1,2x10^{13}$
200 nm	$1,8x10^{12}$
500 nm	$2,5x10^{11}$
1000 nm	$5,4x10^{11}$

Aged	50 µg/mL
100 nm	$1,2x10^{13}$
200 nm	$2,1x10^{12}$
500 nm	$3,5x10^{11}$
1000 nm	$2,0x10^{12}$

Million particle per cell

96-well

Pristine	12,5 µg/mL	25 µg/mL	50 µg/mL	100 µg/mL	200 µg/mL
100 nm	11.8	23.5	47.1	94.1	188.2
200 nm	1.8	3.5	7.0	14.0	28.0
500 nm	0.3	0.5	1 .0	2.0	4.1
1000 nm	0.5	1.1	2.2	4.3	8.6

Aged	12,5 µg/mL	25 µg/mL	50 µg/mL	100 µg/mL	200 µg/mL
100 nm	11.9	23.8	47,5	95.1	190.2
200 nm	2.1	4.2	8,4	16.8	33.6
500 nm	0.3	0.7	1,4	2.8	5.5
1000 nm	2.0	4.0	7,9	15.9	31.7

12-well

Pristine	50 µg/mL
100 nm	39.2
200 nm	5.8
500 nm	0.8
1000 nm	1.8

Aged	50 µg/mL
100 nm	39.6
200 nm	7.0
500 nm	1.2
1000 nm	6.6

[a]Particle number (Nr.) was estimated based on size distributions obtained by DLS, considering the % of particle from each size as reported by the zetasizer, the density of PCL particles as reported by the supplier, i.e., 1.145 g/cm^3, the volume of exposure medium in each well type (100 µL in 96-well plates and 1 mL in 12-well plates), and the particle mass concentration used in the considered assay (12.5, 25, 50, 100 and 200 µg/mL in 96-well plates for cytotoxicity experiments; 12.5, 25 and 50 µg/mL in 96-well plates for DHR123 assay; 50 µg/mL in 12-well plates for DNA damage assay, IL-8 secretion ELISA assay and RT-qPCR).

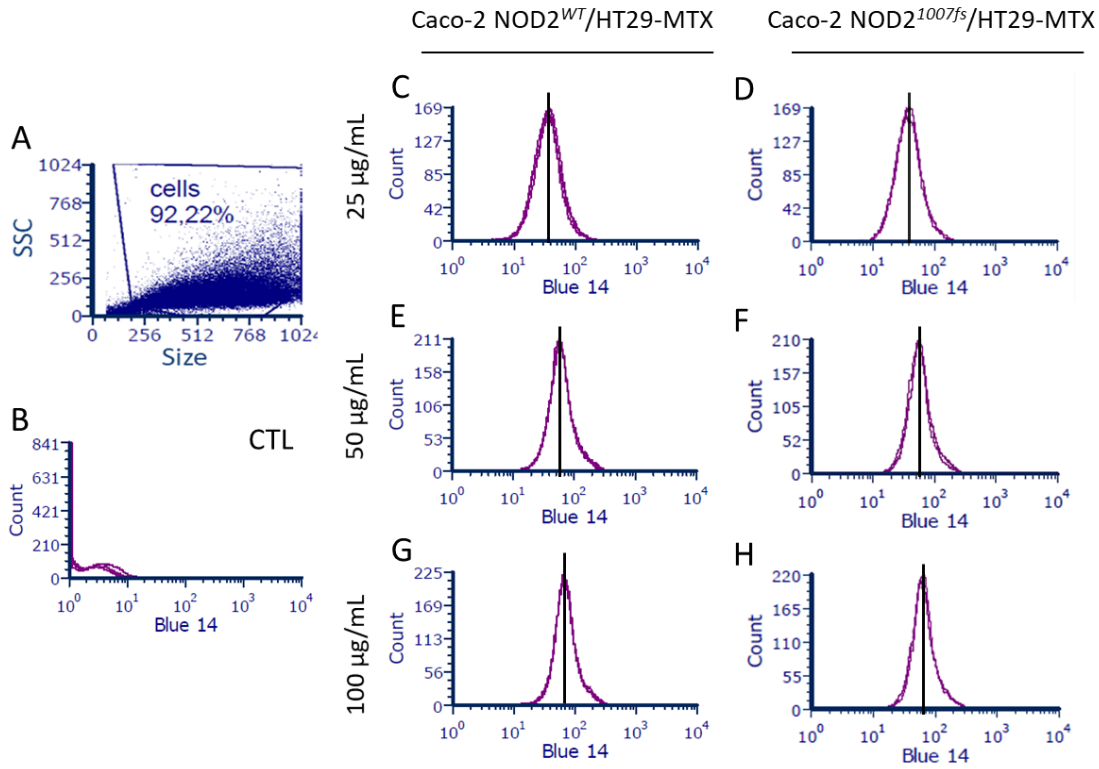

Figure S4. Intracellular accumulation of PCL-DB14 particles, analysed by flow cytometry. (A) gated cells, (B) fluorescence of control (unexposed) cells. (C-H) fluorescence of cells exposed to 25 µg/mL (C-D), 50 µg/mL (E-F), 100 µg/mL (G-H) of PCL-DB14, Caco-2 NOD2^{WT} /HT29-MTX (B, C, E, G) and Caco-2 NOD2^{1007fs} / HT29-MTX (D, F, H).

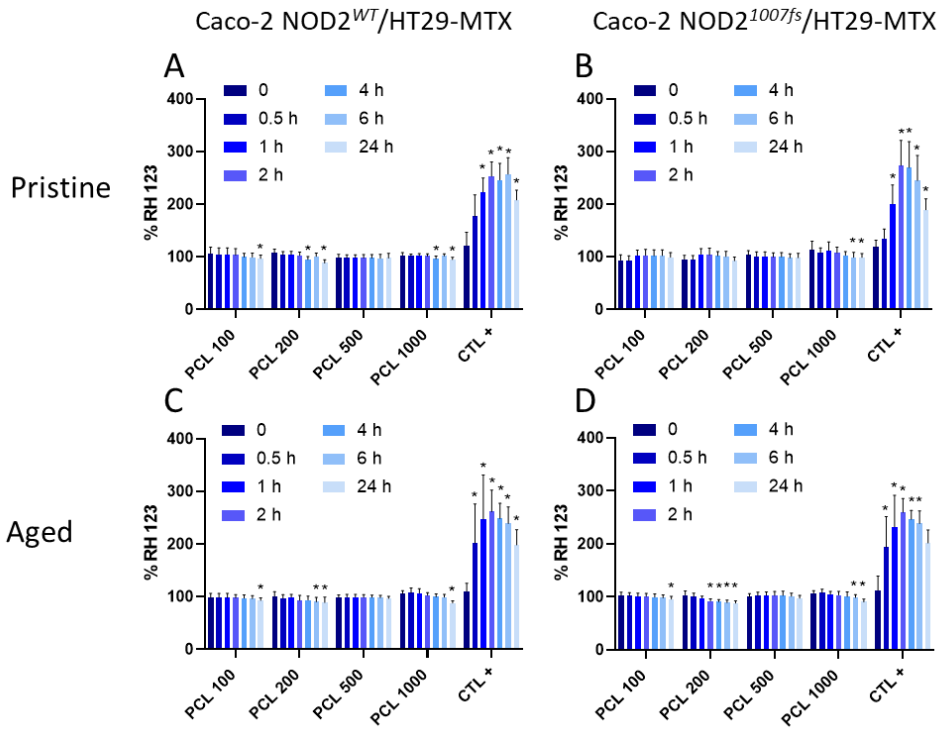

Figure S5. Intracellular ROS level monitored throughout exposure time, in non-differentiated Caco-2 NOD2^{WT} $^{or\ 1007fs}$/HT29-MTX cells. Cells were exposed 24 h after seeding, for 24 h, to 50 µg/mL pristine (A, B) or aged (C, D) PCL particles. Caco-2 NOD2^{WT}/HT29-MTX (A, C) and Caco-2 NOD2^{1007fs}/HT29-MTX (B, D) cells. TBHP (1 mM) was used as positive control. Measurements were recorded immediately after exposure (0), or 0.5 h, 1 h, 2 h, 4 h, 6 h or 24 h post-exposure. Results are expressed as % relative to the control (unexposed cells). Mean ± standard deviation; statistical significance: *p<0.05, exposed vs CTL.

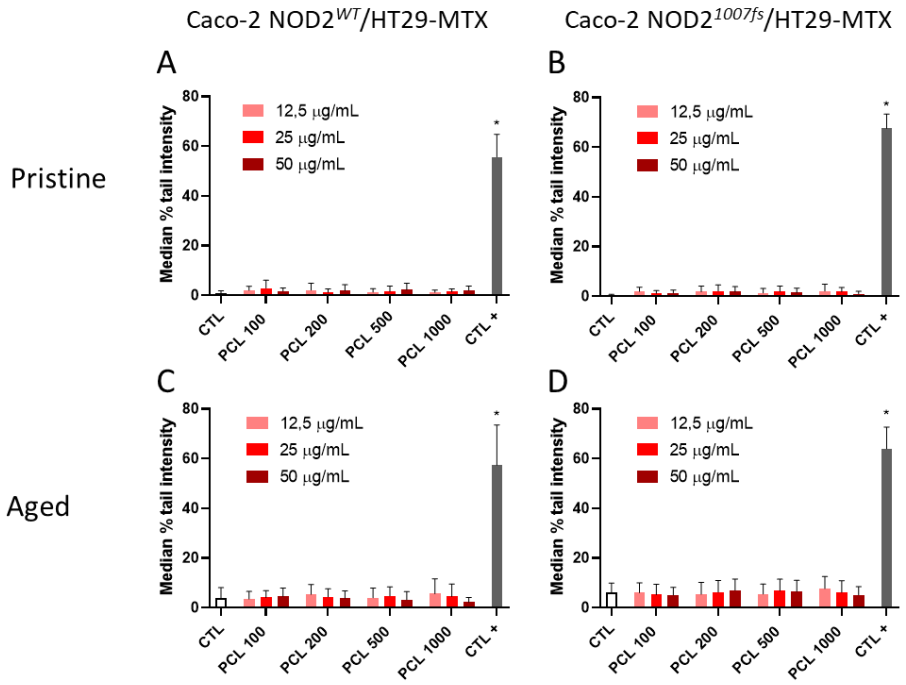

Figure S6. Genotoxicity of PCL particles towards non-differentiated Caco-2 NOD2$^{WT\ or\ 1007fs}$/HT29-MTX cells. Genotoxicity was assessed by the comet assay in alkaline conditions (no Fpg) in cells exposed for 24 h to 12.5 µg/mL, 25 µg/mL or 50 µg/mL of pristine (A, B) or aged (C, D) PCL NPLs. Caco-2 NOD2^{WT}/HT29-MTX (A, C) and Caco-2 NOD2^{1007fs}/HT29-MTX (B, D) cells, exposed 24 h post-seeding. MMS (30 µg/mL) was used as positive control. Results are expressed as %Tail DNA. Mean ± standard deviation; statistical significance: *p<0.05, exposed vs CTL.

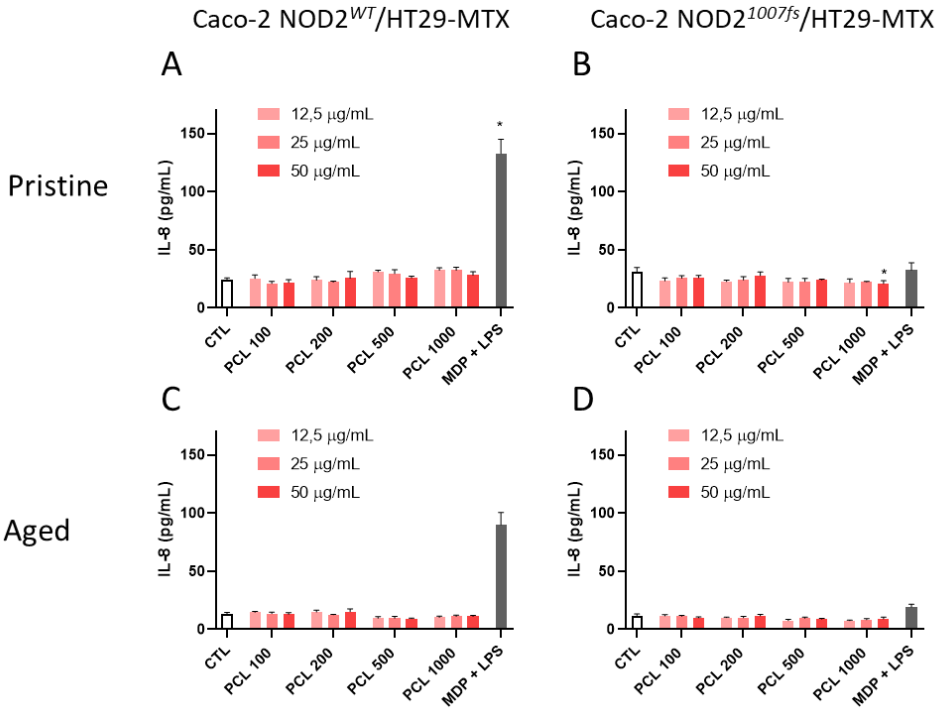

Figure S7. IL-8 secretion by non-differentiated Caco-2 NOD2$^{WT\ or\ 1007fs}$/HT29-MTX cells after exposure to PCL NPLs. IL-8 secretion was assessed using ELISA, in the exposure medium of cells exposed for 24 h to 12.5 µg/mL, 25 µg/mL or 50 µg/mL of pristine (A, B) or aged (C, D) PCL NPLs. Caco-2 NOD2^{WT}/HT29-MTX (A, C) and Caco-2 NOD2^{1007fs}/HT29-MTX (B, D) cells, exposed 24 h post-seeding. A mixture of MDP (10 µg/mL) and LPS (2 µg/mL) was used as a positive control. Mean ± standard deviation; statistical significance: *p<0.05, exposed vs CTL.

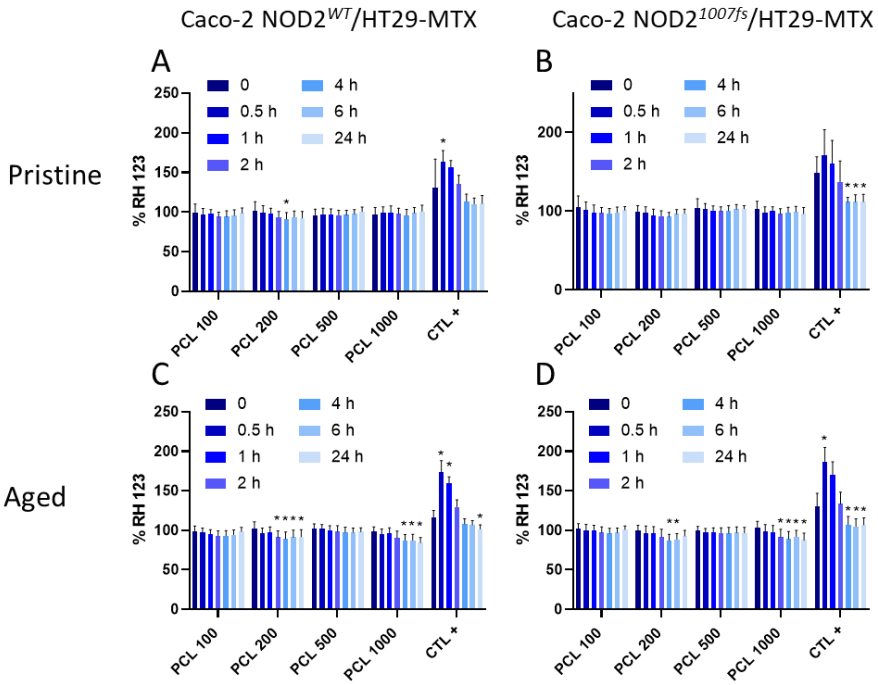

Figure S8. Intracellular ROS level monitored throughout exposure time, in differentiated Caco-2 NOD2$^{WT\ or\ 1007fs}$/HT29-MTX cells. Cells were differentiated 21 days post-confluence, then, they were exposed for 24 h to 50 µg/mL pristine (A, B) or aged (C, D) PCL particles. Caco-2 NOD2^{WT}/HT29-MTX (A, C) and Caco-2 NOD2^{1007fs}/HT29-MTX (B, D) cells. TBHP (1 mM) was used as positive control. Measurements were recorded immediately after exposure (0), or 0.5 h, 1 h, 2 h, 4 h, 6 h or 24 h post-exposure. Results are expressed as % relative to the control (unexposed cells). Mean ± standard deviation; statistical significance: *p<0.05, exposed vs CTL.

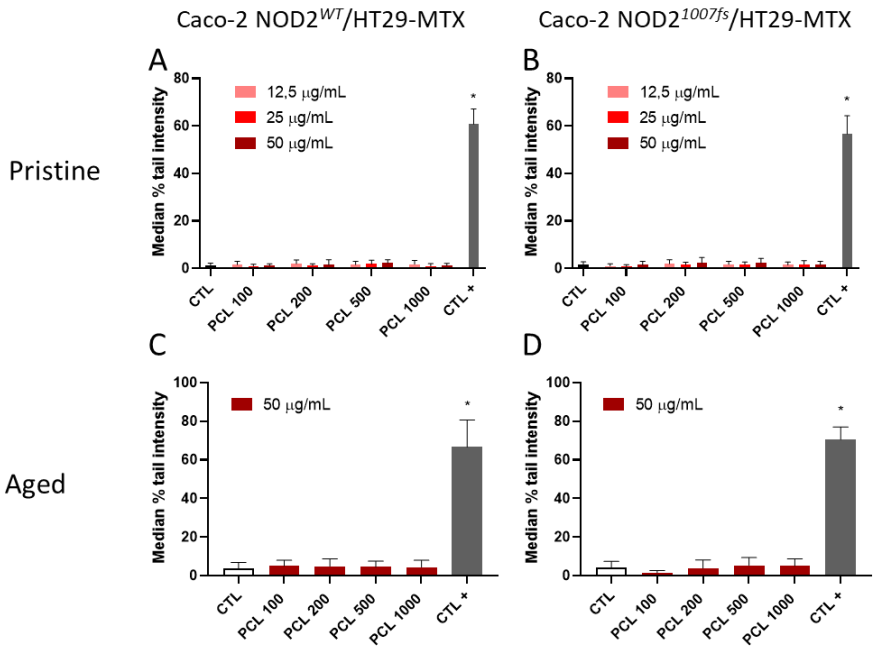

1139

1140 **Figure S9. Genotoxicity of PCL particles towards differentiated Caco-2 NOD2$^{WT\ or\ 1007fs}$/HT29-MTX cells.** Cells
1141 were differentiated by growing them for 21 days post-confluence, before being exposed. Genotoxicity was
1142 assessed by the comet assay in alkaline conditions (no Fpg) in cells exposed for 24 h to 12.5 µg/mL, 25 µg/mL or
1143 50 µg/mL of pristine (A, B) or aged (C, D) PCL NPLs. Caco-2 NOD2^{WT}/HT29-MTX (A, C) and Caco-2 NOD2^{1007fs}/HT29-
1144 MTX (B, D) cells. MMS (30 µg/mL) was used as positive control. Results are expressed as %Tail DNA. Mean ±
1145 standard deviation; statistical significance: *p<0.05, exposed vs CTL.

1146

1147

1148